ISTANBUL TECHNICAL UNIVERSITY ★ ENERGY INSTITUTE

THERMAL HYDRAULICS ANALYSIS OF ITU TRIGA MARK II RESEARCH REACTOR WITH 3D COMPUTATIONAL FLUID DYNAMICS SIMULATION

M.Sc. THESIS

Feride KUTBAY

Nuclear Research Division

Radiation Science and Technology Programme

JULY 2020

ISTANBUL TECHNICAL UNIVERSITY ★ ENERGY INSTITUTE

THERMAL HYDRAULICS ANALYSIS OF ITU TRIGA MARK II RESEARCH REACTOR WITH 3D COMPUTATIONAL FLUID DYNAMICS SIMULATION

M.Sc. THESIS

Feride KUTBAY
(302171001)

Nuclear Research Division

Radiation Science and Technology Programme

Thesis Advisor: Dr. Lecturer Senem ŞENTÜRK LÜLE

JULY 2020

İSTANBUL TEKNİK ÜNİVERSİTESİ ★ ENERJİ ENSTİTÜSÜ

İTÜ TRIGA MARK II ARAŞTIRMA REAKTÖRÜNÜN 3D HESAPLAMALI AKIŞ DİNAMİĞİ SİMÜLASYONU İLE ISIL HİDROLİK ANALİZİ

YÜKSEK LİSANS TEZİ

Feride KUTBAY
(302171001)

Nükleer Araştırmalar Anabilim Dalı

Radyasyon Bilim ve Teknoloji Programı

Tez Danışmanı: Dr. Öğretim Üyesi Senem ŞENTÜRK LÜLE

TEMMUZ 2020

Feride Kutbay, a M.Sc. student of ITU Institute of Energy student ID 302171001, successfully defended the thesis entitled "THERMAL HYDRAULICS ANALYSIS OF ITU TRIGA MARK II RESEARCH REACTOR WITH 3D COMPUTATIONAL FLUID DYNAMICS SIMULATION", which she prepared after fulfilling the requirements specified in the associated legislations, before the jury whose signatures are below.

Thesis Advisor :	**Dr. Lecturer Senem ŞENTÜRK LÜLE** İstanbul Technical University	.....
Jury Members :	**Prof. Dr. Üner ÇOLAK** İstanbul Technical University	.....
	Assoc. Prof. Dr. Şule ERGÜN Hacettepe University	.....

Date of Submission : 15 June 2020
Date of Defense : 13 July 2020

To my Family,

FOREWORD

I am very grateful to my advisor, Asst. Prof. Dr. Senem Şentürk Lüle for sharing her knowledge, for her availability at all time, and for guiding me with patience during my thesis.

I would like to give special thanks to Prof. Dr. Üner ÇOLAK, for his positive and helpful guidance during the study. Many thanks to Assoc. Prof. Dr. Şule ERGÜN for her contributions as jury member.

Special thanks to my family and Ahmet Ertan for their continuous support and motivation.

I would like to thank all my colleagues, especially Fadime Özge Özkan and Sefa Bektaş, for their advice, fruitful discussions, and cooperation.

I would like to give my thanks CNAEM member Yılmaz Peker for technical support.

July 2020

Feride KUTBAY
(Nuclear engineer)

TABLE OF CONTENTS

Page

ABBREVIATIONS

B_4C : Boron Carbide
C : Graphite Reflector
CFD **:** Computational Fluid Dynamics
CHF : Critical Heat Flux
DNS : Direct Numerical Simulation
F4 : Cell Averaged Flux Tally of MCNP Code
FMESH : Superimposed Mesh Tally Card of MCNP Code
ITU : Istanbul Technical University
KCODE : Criticality Card of MCNP Code
KSRC : Criticality Source Definition Card of MCNP Code
LES : Large Eddy Simulation
NEA : Nuclear Energy Agency
NRS : Nuclear Reactor Safety
ONB : Onset of Nucleate Boiling
PRESTO : Pressure Staggering Option
RANS : Reynolds-Averaged-Navier-Stokes
SS : Stainless Steel
3D : 3 Dimensional
TH **:** Thermal Hydraulic
TRIGA **:** Training Research Isotope Production General Atomic
UDF : User Defined Function
UZrH : Uranium Zirconium Hydride
Zr : Zircon

SYMBOLS

α : Alpha Particle
β : ki & thermal expansion coefficient, K^{-1} & thermal conductivity, W $m^{-1}K^{-1}$
β_{eff} : Effective delayed neutron fraction
ϕ : Neutron flux, neutron $cm^{-2}s^{-1}$
$\$$: Reactivity in dollars
E : Energy
ε : Turbulent dissipation rate
F : Body force, g m^{-1} s^{-1}
γ : Gamma rays
g : Gravitational acceleration, m s^{-2}
J_j : Diffusion flux
χ : Fission spectrum
k : Multiplication factor & turbulent kinetic energy
k_{eff} : Effective thermal conductivity W/m-K
μ : Viscosity, kg m^{-1} s^{-1}
ν : Number of neutrons per fission
Ω : Direction
p : Pressure, Pa
P : Power, MW
q''' : Volumetric heat generation. W m^{-3}
q'' : Heat flux, W m^{-2}
r : Position
R : Reaction rate
Ra : Rayleigh number
ρ : Density, kg m^{-3}
S : Scaling factor, W neutron J^{-1}
σ : Microscopic cross section, barn
Σ : Macroscopic cross section, cm^{-1}
T : Temperature, K
t : Time, s
$\vec{u}$: Velocity vector in x-direction, m s^{-1}
v : Velocity, m s^{-1}
$\vec{v}$: Velocity vector in y-direction, m s^{-1}
V : Arbitrary volume, m^3
w_f : Effective energy released per fission, MeV
w/o : Weight percent
x : Cartesian coordinate, m
y : Cartesian coordinate, m
z : Cartesian coordinate, m

Subscripts:

a **:** Absorption
c **:** Clad
eff **:** Effective
f **:** Fission & fuel
g **:** Gap
MC **:** Monte Carlo
m **:** Moderator
sat **:** Saturation
t **:** Turbulent
wall **:** Wall

LIST OF TABLES

Page

LIST OF FIGURES

Page

THERMAL HYDRAULICS ANALYSIS OF ITU TRIGA MARK-II RESEARCH REACTOR WITH 3D COMPUTATIONAL FLUID DYNAMICS SIMULATIONS

SUMMARY

Research reactors on the contrary to power reactors are not used for energy production. However, they play a key role for development of nuclear science and technology and contribute the development of power reactors. In this regard, the primary use of research reactors is to provide a neutron and gamma source through in core and out core positions for research or sometimes for commercial purposes such as radioisotope production. The other important contribution of them is on code development and validation. Indeed, they provide a connection between computational tools and experimental data therefore help the development of codes that are used for design and analysis of nuclear power plants.

From the technical point of view, research reactors are smaller and simpler than power reactors. They usually operate at low temperature and low pressure conditions. In addition, they may contain highly enriched uranium. The energy from fission must be transferred from the fuel to a coolant. The cooling is generally based on natural convection for the low power research reactors whereas the high power research reactors need forced cooling.

Developed by General Atomics, ITU TRIGA Mark II research reactor reached first criticality on March 11, 1979 and serves for training, education, neutron activation, gammagraphy, neutrongraphy, and irradiation. ITU TRIGA Mark II is a 250 kW open pool type research reactor housed in a hexagonal structure providing both structural integrity and biological shield. It can pulse up to 1200 MW for short periods of time. The fuel is specially designed to provide inherent safety to the reactor. Uranium Zirconium Hydride (UZrH) fuel material is in stainless steel cladding. Throughout the core graphite is heavily used for several purposes. There are three beam ports (out-core), central thimble, and pneumatic system (in-core) for irradiation. The reactor control is accomplished by three control rods and reactivity feedbacks.

The general objective of nuclear reactor safety is to protect the safety barriers especially fuel clad integrity which is called the second barrier of defense in depth concept (first barrier being fuel material itself). Several criteria introduced to protect the system. Safety analysis are performed to make sure that these criteria met for normal operation and accidents. Therefore, the safety analysis of nuclear reactors is the most important aspects in the design and safe operation.

The main scope of this thesis is to provide highly accurate 3D solution for neutronics and thermal hydraulic phenomena in ITU TRIGA Mark II research reactor. Since the governing physics of these phenomena are coupled, two solution models based on the governing physics principle should be performed integrally. In this way, the nuclear data and core parameters such as material temperatures, especially the fuel

temperature, and coolant density are calculated as precisely as possible thanks to 3D conjugate heat transfer modelling.

The first analysis performed in this thesis is neutronic analysis. It was performed using Monte Carlo code MCNP 6.2. In this regard, the MCNP 6.2 neutronic model with full core structure (fuel elements, graphite dummy elements, irradiation channels, neutron source element, control rods, thermal column, beam tubes, graphite reflector, and concrete shielding) generated by Asst. Prof. Dr. Senem Şentürk Lüle was modified according to the needs of this thesis. The neutronic calculations were performed with ENDF/B-VII data libraries for continuous energy interactions and S(α,β) kernel scattering tables to treat low energy (< 4 eV) thermal scattering contribution for Hydrogen in Zirconium Hydride (ZrH) and H_2O moderation materials. In order to perform thermal hydraulic simulations, the axial distribution of volumetric heat generation at 250 kW power in each fuel element is necessary. In this regard, cell averaged flux (F4) and superimposed mesh tally (FMESH) features of MCNP code were employed. A second order polynomial was obtained by curve fitting to acquire the axial variation of volumetric heat generation in fuel elements and heat flux at the surface of each fuel elements. These polynomial functions were then inserted as a thermal boundary condition by using UDF feature of FLUENT commercial computational fluid dynamics code for thermal hydraulic calculations.

The second analysis in this study is thermal-hydraulic analysis. The detailed geometry that included pool and core structure was generated to simulate fluid dynamics / heat transfer. However, preliminary simulations showed that this representation was time demanding due to large computational domain. Therefore, the thermal hydraulic investigation had been performed in two separate stages to reduce the computational cost.

At first stage of thermal-hydraulic analysis, the TRIGA pool was modelled by FLUENT version 18.2 to analyze natural convection circulation under steady-state full power operating condition and to predict velocity field and pressure distribution in the core which will be used in the second stage of the thesis. All the components in the core (fuel elements, graphite reflector, thermal column and top and bottom grid plates) were modeled in detail. The calculated coolant temperatures were compared with experimental data from the literature. The results are in good agreement. Furthermore, the effect of grid plates on cooling performance and velocity streamlines in the pool tank was investigated by creating another pool model without grid plates. The grid plate sensitivity analysis showed that grid plates do not have significant influence on temperature distribution. Whereas, the velocity field of pool is reasonably affected from top grid plate. The existence of grid plates reduces coolant velocity at the core exit. As a result, it can be said that the grid plates play role in reduction of dose at top of the pool since they increase the rise time of activation product Nitrogen-16.

At second stage of thermal-hydraulic analysis, only the part inside the reflector was modelled to perform conjugate heat transfer. Therefore, this stage is called as the core model. In this model, heat conduction in fuel elements and natural convection was performed by FLUENT code. The core model was validated and verified with fuel temperature results from instrumented fuel elements at 250 kW power recorded in the logbook of ITU TRIGA Mark II research reactor. The benchmarking showed that, the percent error between simulation and experimental results are below 1 % indicating excellent agreement. Furthermore, the pool boiling phenomenon had been numerically investigated in the core. According to temperature distribution in the core, the pool

boiling curve indicates that the overall flow regime in the core is in single phase or at convective stage. However, the bubble formation occurs locally at some locations on the central fuel elements. The subcooled boiling regime arises at these points.

Finally, the effect of thermal hydraulic parameters on neutronic behavior had been investigated by upgrading the density and temperate of coolant and temperature of fuel elements in MCNP neutronic model according to results of thermal-hydraulic analysis. In this regard, it can be said that the decrease in density of coolant and increase in fuel temperature inserts negative reactivity in the core due to reduction in moderation and Doppler Broadening, respectively.

Unlike previous thermal hydraulic studies that had been performed with major simplifications such as having only 1D, no flow restriction namely no form losses, and no crossflow effects, this thesis offers 3D, fully detailed, validated, and verified neutronic and thermal hydraulic solution. The radial and axial temperature distributions in all 69 fuel elements were provided together with coolant temperature distribution in the tank. Furthermore, modelling of grid plates is out of ordinary since it is usually not performed to provide simplicity.

İTÜ TRIGA MARK II ARAŞTIRMA REAKTÖRÜNÜN 3D HESAPLAMALI AKIŞ SİMÜLASYONU İLE ISIL HİDROLİK ANALİZİ

ÖZET

Nükleer araştırma reaktörleri güç reaktörlerinin aksine elektrik üretimi için tasarlanmamıştır. Ancak, nükleer bilim ve teknolojinin gelişmesinde önemli bir rol oynamakta ve nükleer güç reaktörlerinin gelişimine katkı sağlamaktadır. Bu bağlamda, araştırma reaktörlerinin amacı, bilimsel araştırmalar ve bazen de radyoizotop üretimi gibi ticari kullanımlar için kalp-içi ve kalp-dışı konumlarda çeşitli enerji aralıklarında nötron ve gama kaynağı sağlamaktır. Ayrıca, hesaplama araçları ve deneysel veriler arasında bağlantının kurulmasını sağlayarak, reaktör tasarımında ve analizlerinde kullanılan kodların gelişimine destek olmaktadırlar.

Araştırma reaktörleri güç reaktörlerinden göreceli olarak daha basit ve küçük bir yapıya sahiptir. Genellikle düşük hidrostatik basınç ve düşük sıcaklıklarda çalışırlar. Ayrıca araştırma reaktörlerinde yüksek zenginlikte uranyum içeren yakıt elemanları bulunabilir. Fisyon sonucu ortaya çıkan enerjinin yakıttan uzaklaştırılması için yakıtın bir soğutucu yardımıyla soğutulması gerekmektedir. Soğutma işlemi yüksek güçlü araştırma reaktörlerde cebri soğutma ile sağlanırken, düşük güçteki reaktörlerde ısı doğal taşınım ile kalpten uzaklaştırılabilmektedir.

General Atomics tarafından geliştirilen İTÜ TRIGA Mark II araştırma reaktörü ilk kez 11 Mart 1979 tahinde kritik olmuştur. Araştırma reaktörü eğitim, nötron aktivasyonu, gama radyografisi, nötron radyografisi ve çeşitli ışınlama işlemleri için kullanılmaktadır. İTÜ TRIGA Mark II reaktörü 250 kW nominal ve kısa süreler için 1200 MW darbe güç değerine sahip havuz tipi bir reaktördür. Havuzun bütünlüğünü korumak ve biyolojik bir zırh oluşturmak için altıgen şeklinde bir beton yapı ile reaktör tankı çevrelenmiştir. TRIGA yakıt elemanları kendinden güvenli olacak şekilde tasarlanmıştır. Uranyum Zirkonyum Hidrat (UZrH) yakıt çelik zarf içine konumlandırılmıştır. Reaktör 3 kontrol çubuğu ve reaktivite geri beslemesi ile kontrol edilmektedir.

Nükleer reaktör güvenliğinin genel amacı, güvenlik bariyerlerini, özellikle derinlemesine savunma prensibinin ikinci koruma bariyeri olan (ilk bariyer yakıt malzemesinin kendisidir) radyoaktif ürünlerin yakıt elemanlarının içinde kalmasını sağlayan yakıt zarfının bütünlüğünü sağlamaktır. Sistemi korumak için farklı kriterler oluşturtulmuştur. Güvenlik analizleri bu kriterlerin normal işletmede ve kaza koşullarında sağlanıp sağlanmadığını kontrol eden analizlerdir. Bu nedenle, nükleer reaktörlerin güvenlik analizleri, tasarım ve güvenli işletiminde önemli bir yere sahiptir.

Bu tezin amacı, İTÜ TRIGA Mark II araştırma reaktöründe nötronik ve ısıl hidrolik analizler için son derece hassas 3 boyutlu çözüm sağlamaktır. Reaktör analizlerinde nötronik ve ısıl hidrolik davranışlar birbirine bağlı dinamik yapıya sahiptir. Bu sebeple, tez kapsamında nötronik ve ısıl hidrolik modeller bütünleşik olarak değerlendirilmiştir. Buna istinaden, 3 boyutlu nötronik ve eşlenik ısıl hidrolik

modellemeleri sayesinde nötronik parametreler ile birlikte yakıt elemanlarının sıcaklık değerleri, soğutucu sıcaklık, hız ve basınç değerleri yüksek doğrulukta hesaplanmıştır.

Öncelikle, Monte Carlo olasılıklı yöntemi ile benzetimler gerçekleştiren MCNP 6.2 kodu ile İTÜ TRIGA Mark II araştırma reaktörünün Dr. Öğretim Üyesi Senem Şentürk Lüle tarafından yapılan doğrulanmış 3 boyutlu nötronik modellemesi tez kapsamındaki ihtiyaçlar için yeniden düzenlenmiştir. Geometrik model yakıt elemanları, grafit elemanlar, ışınlama kanalları, nötron kaynağı, kontrol çubukları, termal kolon, ışınlama tüpleri, grafit reflektör ve koruyucu beton olmak üzere detaylı bir şekilde tüm reaktör bileşenlerini içermektedir. Ayrıca, nötronik hesaplamalarda nötron etkileşimleri için tesir kesiti olarak devamlı enerji aralığında ENDF/B-VII veri kütüphanesi ve düşük enerji (< 4 eV) aralıklarında nötronların hidrojen atomu ile saçılma davranışlarının nötronik hesaplamaya dâhil edilmesi için S(α,β) kernel saçılma tabloları kullanılmıştır. Isıl hidrolik hesaplarında kullanılmak üzere farklı güç üreten her bir 69 yakıt elemanında eksenel yönde hacimsel güç dağılımı hesaplanmıştır. Bu hesaplamalarda, MCNP 6.2 kodunda bulunan örgü ağı oluşturmayı sağlayan FMESH özelliği ve üretilen ortalama akıyı veren F4 aracının birlikte kullanılması ile sonuçlar elde edilmiştir.

Tezin ikinci kısmını İTÜ TRIGA Mark II araştırma reaktörünün ısıl hidrolik analizi oluşturmaktadır. Gerçekçi bir analiz için detaylandırılmış kalp ve havuz geometrisi oluşturulmuştur. Ancak, ilk simülasyon denemelerinde havuz ve detaylandırılmış kalp geometrisinin hesaplama örgüsü çok fazla eleman içerdiği için hesaplamaların çok uzun süreceği görülmüştür. Bu nedenle, herhangi bir basitleştirme olmaksızın İTÜ TRIGA Mark II reaktörünün ısıl hidrolik hesaplamalarının iki ayrı model ile gerçekleştirilmesi tercih edilmiştir.

Isıl hidrolik analizlerin ilk aşamasında, TRIGA havuz modeli denge koşullarında 250 kW tam güçte modellenmiştir. Havuz içindeki tüm kalp elemanları (yakıt elemanları, grafit reflektör, termal kolon ve destekleyici alt ve üst plakalar) detaylı bir şekilde modellenmiştir. Havuz modelinin FLUENT sürüm 18.2 kodu ile sayısal çözümü vasıtasıyla havuz tipi TRIGA reaktöründe doğal taşınım ile ısı transfer mekanizması incelenmiştir. Ayrıca, havuz modeli hesaplamalarından ısıl hidrolik analizlerin ikinci aşamasında oluşturulacak kalp modelinde kullanılmak üzere kalp girişi hız dağılımı ve kalp çıkışı basınç dağılımı elde edilmiştir. Hesaplanan soğutucu sıcaklıkları İTÜ TRIGA reaktöründe yapılmış olan deney sonuçları ile karşılaştırılmış ve hesaplanan değerler ile deneysel verilerin uyum içeresinde olduğu görülmüştür. Ek olarak, kalbin alt ve üst kısmında bulunan kalp içi elemanların yerinde kalmasını sağlayan destekleyici plakaların soğutma performansı ve hız dağılımı üzerindeki etkisi incelenmiştir. Bu analize göre, destekleyici plakaların sıcaklık dağılımı üzerinde belirgin bir etkisi gözlenmemiştir. Ancak, havuzdaki hız profili üst destekleyici plakadan belirgin şekilde etkilenmektedir. Destekleyici plakaların havuz içinde bulunması kalp çıkışında hızı düşürmektedir. Sonuç olarak, destekleyici plakalar aktivasyon ürünü Azot-16'nın havuzun üst kısmına ulaşma süresini arttırdığı için buradaki dozun azaltılmasında rol oynamaktadır.

Isıl hidrolik analizlerin ikinci aşamasında, yakıt elemanlarındaki sıcaklık dağılımını bulmak üzere sadede reflektörün iç kısmı modellenmiştir. Bu sebeple bu model kalp modeli olarak adlandırılmıştır. Bu model İTÜ TRIGA Mark II araştırma reaktörünün işletme kayıtlarındaki 250 kW güçteki yakıt sıcaklık değerleri ile doğrulanmıştır. Kıyaslama, simülasyon ve deneysel sonuçların %1'in altında bir fark ile mükemmel bir uyum aralığında olduğunu göstermiştir. Ayrıca tez kapsamında, TRIGA havuzunda

havuz tipi kaynama sayısal yöntemler ile incelenmiştir. Kalp içindeki sıcaklık dağılımına göre, havuz tipi kaynama eğrisi kalp içi genel akış rejiminin tek fazlı olduğunu, fakat kalp merkezindeki yakıt elemanların bazı noktalarında kabarcık oluşumu gözlendiğini göstermiştir. Bu sebep ile bu bölgelerde kaynama-altı kaynama gerçekleşmektedir.

Son olarak, ısıl hidrolik parametrelerinin nötronik davranış üzerindeki etkisi araştırmak üzere ısıl hidrolik analizlerden elde edilen soğutucu ve yakıt sıcaklıkları kullanılarak MCNP nötronik model geliştirilmiştir. Bu bağlamda, soğutucu yoğunluğundaki azalmanın ve yakıt sıcaklığındaki artışın sırasıyla yavaşlatma kapasitesindeki azalma ve Doppler genişlemesi nedeniyle kalbe negatif reaktivite eklediği söylenebilir.

Bu tez çalışması, İTÜ TRIGA Mark II reaktöründe daha önce yapılmış pek çok basitleştirmeyi içeren, tek boyutlu, akış geçişlerindeki geometrik etkilerin göz önüne alınmadığı ve yanal akışların hesaba katılmadığı çalışmaların aksine, reaktörün detaylı bir şekilde modellendiği, 3 boyutlu (3B) ve doğrulanmış ilk çalışma olmuştur. 69 yakıt elemanının tamamında radyal ve eksenel yönde sıcaklık dağılımları ile tank içindeki soğutucu sıcaklık dağılımı hesaplanmıştır. Ayrıca, genellikle hesaplamaları basitleştirmek için ihmal edilen alt ve üst destek plakalarının bu çalışmada modellenmesi çalışmaya özgünlük katmaktadır.

1. INTRODUCTION

The research reactors have been the most important milestones of the development of the nuclear science and technology. Research reactors offer a wide range of applications such as radioisotope production, neutron beam research applications for testing and developing materials to be used in nuclear applications and commercial nuclear reactors, and education and training. In addition, they provide services for code development and validation by connecting computational tools with the experimental data.

There are several different types of research reactors that are designed and build for dedicated purposes. Therefore, they provide tremendous amount of freedom in design such as having high or low neutron flux, using light water or heavy water as coolant, being pool type or vessel type, having various irradiation facilities in-core and out-core or having cylindrical or plate type fuel elements etc. ITU TRIGA Mark II research reactor is one of these types developed by General Atomics. It is a tank type research reactor confined in a hexagonal structure that provides both structural integrity and biological shielding. The fuel is specially designed to provide inherent safety to the reactor. Uranium Zirconium Hydride (UZrH) fuel material is placed in stainless steel cladding. Throughout the core Graphite is heavily used as reflector in the core and moderator in the thermal column. There are three beam ports for out-core irradiation and central thimble and pneumatic system for in-core irradiation. The reactor control is accomplished by three control rods and reactivity feedback coefficients. It is used since 11 March 1979 for education and training, neutron activation analysis, gammagraphy and neutrongraphy, and irradiation purposes.

The safety of nuclear reactors either research or commercial is the most important aspect in design and operation. The safety concept includes both neutronic and thermal hydraulic limits. Therefore, calculations are necessary to make sure that these limits are not exceeded. Regarding neutronic calculations, complex neutron transport equations for different geometries and materials must be solved. Regarding the

thermal hydraulics calculations, the governing equations of conservation of mass, momentum and energy must be solved again for complex geometries. These two tasks are not easy to handle. Because of that, at the first phase of nuclear technology development, preliminary knowledge base and extreme assumptions were used. The operating experience and experimental studies in pilot facilities later used for advancement in computational methods and empirical correlations. In following years, reliable simulation codes in both fields were developed (WIMS, CITATION, MCNP, SCALE, SERPENT, etc.) for neutronic calculations and (COBRA, RELAP, CATHARE, ATHELETE, MARS, TRACE, etc.) for thermal hydraulic calculations [1]. Nuclear Energy Agency (NEA) describes the method of modelling in system codes that couple neutronic and thermal hydraulic analysis such that whole primary circuit is described by constructing one dimensional approach for tubes, zero-dimensional approach for some supplementary components such as lower and upper plenum, water tank; pump etc., and homogenized three-dimensional approach for the core [2].

The system codes can solve fluid equations conjugate with solid conduction for steady state and transient simulation. In case of transient condition, the solution includes neutron kinetic equations with feedback effects. Traditional approach system codes do not have capability to solve turbulent diffusion in flow. Instead of taking into account contributions of the turbulent dissipations directly, the empirical correlations for the heat transfer and friction coefficients for pressure drop are employed. The correlations are well validated mostly for 1D calculations thus they may restrict the use of system codes to demonstrate full flow characteristics in complex geometries such as the lower and upper plenum, downcomer, mixing spacer grid in reactor core. In this respect, thermal hydraulic studies have focused on newly developed system codes and computational fluid dynamics (CFD) codes which are capable of handling three-dimensional complex geometry and two-phase flows.

The development in computer technology in recent years lead increased computing power with fast multi-core processors and high memory capacity. These allow multi-dimensional multi-physics realistic modelling in nuclear technology design and analysis. In this regard, the early use of CFD in the nuclear reactor safety (NRS) field aimed to accumulate verified and validated experiences in this area by technical reports of NEA [3]. On the other hand, in recent years, three-dimensional and multi-physics simulations are widely used by safety specialist and reactor designers for detailed

information on heat transfer and evaluation flow behaviors in nuclear reactor core. Here, multiple physics approaches for nuclear reactor modeling are based on a fully integrated solution of neutronic-thermal-hydraulics and thermo-mechanical phenomena, as opposed to traditional nuclear reactor analysis which includes separate assessment of different phenomenological effects.

The comprehensive high-fidelity reactor core modeling developed by the US-ROK stakeholders of the I-NERI Project[1] is a pioneering study in the multi-physical model [4], [5]. The motivation of this study is to provide highly refined coupled solution of neutronic, thermal-hydraulic, and thermo-mechanical phenomenon for the design of advanced reactors. In this regard, neutron transport was simulated with De-CART code (Deterministic Core Analysis based on Ray Tracing), thermal hydraulics was simulated with STAR-CD, CFD-ACE and CFX commercial codes (fluid dynamics and conjugate heat transfer) with very fine mesh domain and finite element based thermo-mechanics was simulated with NEPTUNE code.

In this thesis, neutronic thermal-hydraulic analysis of ITU TRIGA Mark II research reactor was performed by coupling MCNP (version 6.2) Monte Carlo code for neutronic and FLUENT (version 18.2) CFD code for thermal hydraulics. Reactor coolant temperature distribution in the pool and fuel axial and radial temperature distribution for all 69 fuel elements were calculated. The verified methodology used and corresponding results were discussed in several sections of the thesis.

The methodology applied for simulations and the details of the results are a first for ITU TRIGA Mark II research reactor. The methodology of including the effect of grid plates that hold the fuel elements in place in the core is the uniqueness of this study because in general for simplicity grid plates are not modeled although they have significant effect on coolant velocity field.

[1] The project was sponsored by International Nuclear Energy Research Initiative (I-NERI) and high-fidelity core design tool is developed by colleagues from Korea Atomic Energy Research Institute (KAERI), Purdue University, and Seoul National University [5].

2. LITERATURE REVIEW

The determination of neutronic parameters of nuclear reactors is essential for safe operation and design. With advanced computing opportunities, the neutronic studies have focused on the Monte Carlo method due to its capability of modelling 3D complex geometries without any major simplifications. The first neutronic analysis based on the Monte Carlo approach for ITU TRIGA Mark II reactor is initiated by the use of SCALE radiation transport code to overcome limitations of special one-dimensional TRIGA codes such as TRIGAP [6]. In that work, the excess reactivity and control rod worth were assigned with KENOva module in the SCALE code. Furthermore, 3D neutronic core modelling was carried out to determine the neutronic parameters of the ITU research reactor by Turkmen et al., such as the effective core multiplication factor, k_{eff}, the excess reactivity, ρ_{excess}, control rod worth, power peaking factors, effective delayed neutron fraction, β_{eff}, using MCNP5 code [7].

The one or two dimensional numerical and experimental analysis conducted with thermal hydraulic (TH) phenomena were achieved in ITU Nuclear Energy Institute. In the Özkul's master thesis [8], the one dimensional thermal hydraulic analysis was performed by indigenous FORTRAN program code based on control volume approach and SIMPLE solution algorithm. Furthermore, it was assumed that the TRIGA core consists of individual rod-centered subchannels. The coolant and fuel temperature as well as coolant velocity and pressure distribution along the channels were calculated for B1, C1, D1, E1, and F1 subchannels assuming that there is no heat and momentum transfer between the channels. The mixed (natural and forced) convection correlations were used to achieve convective heat transfer for steady and transient flow regimes. According to the results, the maximum fuel temperature at the B1 fuel element was calculated as 223 °C at 250 kW full power [9].

Time dependent two-dimensional simulation based on coupled neutronic and thermal hydraulic models were developed by Özkan within the scope of a master thesis [10]. Regarding the neutronic modelling, two-dimensional time dependent coupled nodal

kinetic equations based on neutron perturbation theory was numerically solved using semi-implicit techniques. Furthermore, the reactivity insertion to kinetic equations provided by the control rod worth and temperature reactivity feedback coefficient. In the thermal hydraulic model, the temperature of fuel elements was calculated only in axial direction assuming fuel elements have no zirconium rod, no clad and no graphite plugs parts besides convection term of heat transfer mechanism was provided by calculating heat transfer coefficient using Blasius equation. Another related study conducted with coupled kinetic neutronic and thermal hydraulic modelling was introduced by Can et al. [11]. In this study, the discretized governing equations was corrected by Hansen method.

The experimental and analytical study on ITU TRIGA Mark II were performed by Buke and Yavuz [12]. In this study, the coolant temperature in the core at different power levels was measured by inserting a portable thermocouple through the foil insertion holes. At the same time, fuel temperature results were recorded during the experiment. Moreover, the B1 instrumented fuel was shuffled to measure fuel temperature at two different locations in rings B, C, D, E and F for different reactor powers. Furthermore, an in-house FORTRAN-77 code which solves heat conduction problems in two dimensions (r, z) at steady state condition was developed. This computer program was verified with the experimental data. The calculated results were in fairly good agreement with the experimental data.

The system codes such as ATHLET, CATHERE, RELAP, and RETRAN are widely used in nuclear engineering and design to estimate thermal hydraulic parameters under normal and accidental conditions. These codes utilize some correlation to calculate convective heat transfer coefficient, pressure drop originated friction and geometrical changes (expansion, contraction, elbows etc.). In the last few years, instead of one or two-dimensional system codes, the trend is to switch to 3D realistic methods such as computational fluid dynamics which allows highly refined numerical modelling of various flow and heat transfer problems.

CFD techniques is widely used in early phase of a certain design to understand underlying physics. Thus, CFD simulations play a key role in terms of prefeasibility studies and conceptual clarification. These simulations usually include a relatively large domain and multi-physics models (whole assemblies and involve neutronic coupling).

A feasibility study was performed on power upgrading of the university of Utah TRIGA reactor to investigate the thermal-hydraulics and heat transfer characteristics in respect to cooling and system requirements and design [13], [14]. In this study, natural convection circulation at TRIGA was simulated by CFD codes ANSYS Fluent and SolidWorks and a system code PARET ANL. The power level of the TRIGA simulations was increased from 90 kW to 500 kW to determine a new design for the increasing power. It was found that nucleate boiling arises at 210 kW and flow did not approach the CHF (Critical Heat Flux) up to 500 kW. The study estimated that the total cost of the replacement of cooling system when the operational power is upgraded to 210 kW is $180.000.

Another design basis research was carried out by Nazar et al. [15]. The study aimed to determine whether the RSG GAS reactor's plate type fuel elements (MTR) could be used in TRIGA reactor core instead of General Atomic TRIGA plate type fuel elements since the General Atomic no longer produces TRIGA 2000 fuel elements. Therefore, Bandung TRIGA 2000 research reactor with MTR type fuel elements was modeled using CFD code Fluent. The results of CFD simulations demonstrate that the pure convection conditions did not satisfy the operational safety conditions. Thus, the forced convection cooling was modelled at different flow rates. According to the results of forced convection simulations, the coolant flow rate at the core inlet must be greater than 50 kg/s.

A CFD model of the Brazilian IPR-R1 TRIGA research reactor pool including core elements was developed using Ansys CFX code by Lianes et al. [16]. In this study, the steady-state mixed flow simulation was performed at 50 kW power level. Meanwhile, the mixed convection was set up by buoyancy effects conducted with temperature dependent coolant density and inlet velocity condition on inlet pipe. The results of the study showed that the temperature difference between the core inlet and outlet was about 5 °C at 50 kW reactor power.

To provide a different perspective, a CFD analysis on IPR-R1 TRIGA research reactor was achieved by Vitor V. et al. using an open source CFD code OPENFOAM [17]. The study preferred to model representative subchannels; triangular subchannel, quadrangular subchannel, and one near the reactor wall called reflector subchannel instead of whole core to check the temperature difference and effects of cross flow. The extreme assumptions caused that the results were strongly disagree with the

experimental data since the heat flux of fuel rod surface was considered equal and there was no physical representation of cross flow and natural convection.

In nuclear safety concept, the design criteria of fuel element refer to maintain fuel integrity during normal and off-normal conditions. This is strongly related to capacity of heat removal system to cool the fuel elements under normal/off normal conditions as well as after shutdown. In this regard, thermal-hydraulic design limits for nuclear reactors such as the maximum fuel and clad temperature, maximum linear heat generation rate, the minimum departure from nucleate boiling, the minimum critical power ratio should be set in sufficient safety margins in operating conditions for fuel integrity and prevention of release of radioactive materials to environment [18]. Regarding the TRIGA fuel design limits, the maximum fuel temperature limit depends on the Hydrogen content in UZrH and varies between 1000 °C and 1100 °C whereas the maximum clad temperature limit is around 500 °C [19].

In the thermal hydraulic analysis, conjugate heat transfer analysis provides the information whether maximum fuel and clad temperatures are below their allowable limits. Here, conjugate heat transfer analysis involves the solution of coupling between the conduction in the fuel elements and the convection in the coolant by satisfying the conditions of continuity in temperature and heat flux at the fuel–coolant interface. Thermal hydraulic studies have mostly focused on best estimate methods with state of the art multi-physics approach in recent years.

A preliminary study on coupled neutronic analysis with Monte Carlo approach and thermal hydraulic analysis with CFD methods was introduced by Şeker et al. [20]. In that study, 3x3 PWR pin cell was simulated by a computational code system based on Monte Carlo neutron transport code MCNP5 and CFD code STAR-CD and nuclear data generation code NJOY. In this regard, an interface computer program called McSTAR was developed by FOTRAN90 programming which has ability to internally couple MCNP5 and STAR-CD codes by changing temperature and density data between the codes and update cross-section library in MCNP5. The results were benchmarked high fidelity multi-physics calculation that was performed deterministic neutron transport code DeCART and STAR-CD CFD code [5]. The coupled calculation results demonstrated that the effective criticality and power profile is in good agreement. In addition, this preliminary study showed that the Monte Carlo and CFD coupling methodology is feasible for reactor calculations.

The similar study based on coupling Monte Carlo/CFD methodology was performed at University of Illinois by Cardoni and Uddin [21]. In this study, the incorporated neutronic and thermal hydraulic analysis of a PWR fuel pin cell performed using MCNP5 and STAR-CCM+ codes. Furthermore, the temperature dependent nuclear data, Doppler broadened resolved resonance data and S(α,β) kernel scattering data were generated by MAKXSF utility code of MCNP5. The simulations were run separately and coupled externally by means of Perl scripts which automatically exchanged temperature, density, and volumetric heating information between the codes. The coupled results showed the realistic power distribution, fuel temperature distribution, and adequate fluid characteristics for a simple PWR pin-cell.

The novel multi-physics approach based on coupling of neutronic and thermal hydraulic phenomenon was applied on TRIGA Mark II research reactor at Jozef Stefan Institute by Henry Romain in his Doctoral thesis [22]. In this study, the neutronic calculations were performed using Monte Carlo code TRIPOLI and verified with MCNP5 code. In thermal hydraulics part of the thesis, the natural convection flow in pool simulated by CFD code ANSYS CFX and then the conjugate heat transfer analysis was performed to model TRIGA core region. Furthermore, the temperature dependent nuclear data was generated by NJOY nuclear processing code. A steady state coupling of neutronic/ thermal hydraulic was carried out by exchanging thermo-fluid data and fuel temperature.

3. THEORY

3.1 Reactor Physics

3.1.1 Neutron transport theory

Neutron populations are governed by neutron interactions throughout the medium with scattering, capture, and fission occurrence. There are several physical expressions for the representation of neutron behavior in a medium. Boltzmann for example introduced a statistical mechanistic formulation to describe interaction of gases in a medium that is used for the description of neutron behavior in a nuclear reactor. There are several forms of neutron transport equations which are described in [23] as the Green's function form, The Pseudo equation, the integral equation as well as the different detailed solution approaches for the different form for neutron transport equations introduced by Duderstadt [24]. In this thesis, the Boltzmann neutron transport equation in integro-differential form is used to describe the diffusion of neutrons through a medium since it is widely used in reactor physics applications.

In the Boltzmann transport formulation, the prediction of neutron population is governed by gain and loss rates which are determined by neutron interactions within the medium. In this regard, each neutron is specified by 6-dimensional space including time (*t)*, position *r(x,y,z)*, velocity (*v*) or energy (*E*), and direction (Ω) which is defined as $v/|V|$. Contributions to total number of neutrons within an arbitrary volume *V* are specified as partial space element $\Delta\Omega\Delta E$ during a time Δt are shown in Figure 3.1.

$$\begin{bmatrix}\text{Number at}\\ \text{time } t+\Delta t\end{bmatrix}=\begin{bmatrix}\text{Number at}\\ \text{time } t\end{bmatrix}+\begin{bmatrix}\text{Number gained}\\ \text{during } \Delta t\end{bmatrix}-\begin{bmatrix}\text{Number lost}\\ \text{during } \Delta t\end{bmatrix}$$

Figure 3.1 : Neutron balance specified by partial element $\Delta\mathbf{\Omega}\Delta\mathbf{E}$ within a volume.

All contributions to neutron balance in an arbitrary volume *V* are grouped according to gain or loss mechanisms and each term can be represented by a differential partial element. In this respect, the mathematical expressions for each gain and loss

mechanisms in terms of angular density *n(r,E,Ω,t)* is possible [25]. From physics point of view, neutron gain can be accomplished by

- External neutron source in volume *V*,
- Fission,
- Streaming into volume *V* through the surface *S*,
- Scattering gain.

The loss mechanisms can be:

- Leakage out through the surface *S*,
- Losses due to scattering and absorption.

The Neutron Boltzmann equation including aforementioned contributions is given in Equation 3.1.

$$\int_V dr \left\{ \begin{array}{l} \left[\frac{1}{v}\frac{\partial}{\partial t} + \Omega.\nabla + \sum(r,E,t) \right] \phi(r,\Omega,E,t) - \\ \int_0^\infty dE' \int_{4\pi} d\Omega' \sum_s (r,\Omega'.\Omega,E' \to E) \phi(r,\Omega',E',t) - \\ \int_0^\infty dE' \int_{4\pi} \frac{\chi(E)}{4\pi} d\Omega' \nu(E) \sum_f (r,E',t) \phi(r,\Omega',E',t) \end{array} \right\} = 0 \quad (3.1)$$

The Equation 3.1 can be solved by deterministic methods numerically. In this thesis however, neutron transport equation is not solved directly but neutron transport is satisfied by stochastically simulating the behavior of neutrons through medium.

3.1.2 The Monte Carlo Method

The transport equation can be solved by means of either numerical or analytical methods for the determination of the specified angular neutron density. However, particle collision events are inherently stochastic in nature; therefore, the Monte Carlo method offers a different approach to simulate the particle transport process directly on a computer without any dispatching the transport equation.

The main idea of random sampling or Monte Carlo method in neutronic studies is to track out neutrons from birth (by fission, external neutron source, etc…) to their death (by absorption, capture, leakage, etc…) while recording interactions they make. Hereof, the number of neutron histories are simulated by several random estimators

such as probability distribution of scattering angles for collision, track length for streaming through the surface. Thanks to using of this method, the sophisticated algorithms has been developed by advanced programming. By this way, Monte Carlo computer codes can simulate tens of thousands of particle histories in complex three-dimensional geometries with detailed treatment of space, energy, and time dependent transport phenomena.

3.1.2.1 Monte Carlo transport code MCNP

MCNP, a general-purpose Monte-Carlo-N-Particle code is widely used to solve neutron, photon, electron or coupled particle transport equations [26]. The code treats any three-dimensional complex geometry by tracking the behavior of sufficient number of particles. In neutronic studies, MCNP code provides estimation of not only multiplication factor (k_{eff}) but also the reaction rates, neutron fluxes and spectra, and power peaking factors etc. Within the scope of this thesis, criticality, reaction rates, and nuclear data features of the code are used.

3.1.3 Criticality Calculation

In the criticality calculations, MCNP code tracks finite number of neutrons, N_o, from their birth via fission to their death via absorption or leakage. The next cycle separated with a number, N_1, fission neutrons weighted by (N_0/N_1). The multiplication factor k_{eff} is defined as the ratio between the number of neutrons in two sequential generations. The multiplication factor can be express as in Equation 3.2.

$$k_{eff} = \frac{\int_V dV \int_{4\pi} d\Omega \int_0^\infty dE \int_{4\pi} d\Omega' \int_0^\infty \frac{1}{4\pi} \chi(E,E') \nu(E') \Sigma_f(r,E') \phi_{MC}(r,\Omega',E') dE}{\int_V dV \int_{4\pi} d\Omega \int_0^\infty \nabla\Omega \phi_{MC}(r,\Omega,E) dE + \int_V dV \int_{4\pi} d\Omega \int_0^\infty \left[\Sigma_a(r,E) + \Sigma_m(r,E)\right] \phi_{MC}(r,E,\Omega) dE} \quad (3.2)$$

where the numerator is neutron production that is fission term represented by fission neutron spectrum $\chi(E, E')$, number of neutrons per fission $\nu(E)$, and the macroscopic fission cross section Σ_f. Specifically, the number of neutrons per fission is energy dependent. However, in thermal reactors or multiplying systems, this dependency can be ignored since fissions occurs in thermal energy range. Therefore, in order to evaluate heat generation along the fuel elements, the average number of neutrons per fission $<\nu>$ is taken account within the thesis. The denominator terms symbolize the neutron losses caused by leakage and neutron absorption, respectively.

In MCNP code, criticality calculation starts by applying source neutrons into the problem. The sources are given with KCODE card and initial spatial neutron distribution is given using the KSRC card, the SDEF card or SRCTR file.

3.1.3.1 Nuclear data

Induced neutrons may undergo different interactions such as scattering, fission, and capture. The possibility of interacting with the target nuclei is represented by microscopic cross-sections. In this respect, all reactions are given in a particular evaluated cross section data base; for instance, ENDF/B-(VIII, VII, VI, and V), JEFF-3.3, 3.2, and JENDL. The data base contains evaluated core nuclear reaction cross sections, fission product yields, angular distributions, photo atomic nuclear data, and thermal scattering law data. MCNP code uses ENDF/B series in raw and ACE formats. ACE format data can be generated by NJOY [27] nuclear data processing system.

" *Eight class nuclear data tables exist for MCNP*" [26]. Continuous energy interaction data and neutron $S(\alpha,\beta)$ thermal data tables are used for neutronic modelling within the thesis. Continuous energy cross section data is available for elastic scattering, fission, inelastic scattering, (n,xn), (n,γ), and various other kinds of absorption reactions. When neutrons are transported to sufficiently low energies, molecular binding effects become important. In this case, thermal $S(\alpha,\beta)$ scattering law data is appropriate for bound scatters such as Graphite, water, Hydrogen in Zirconium, and Beryllium. Therefore, $S(\alpha,\beta)$ thermal treatment is applied in this thesis to consider inelastic scattering in the Zirconium Hydride and H_2O molecules within the MCNP neutronic modelling.

3.1.3.2 Normalization of neutron flux and reaction rates

In criticality calculations, MCNP output tallies give normalized value per source neutron for neutron fluxes and reaction rates. To get corresponding values for measured flux, the scaling constant must be taken into account in calculations.

The neutron flux ϕ_{MC} in MCNP represents neutrons of one generation and the corresponding flux ϕ as a measurable quantity can be calculated by Equation 3.3 [28].

$$\phi = S.\phi_{MC} \tag{3.3}$$

where *S* represents the scaling factor and it is the same for neutron flux and reaction rates. The neutron flux ϕ_{MC} describes the neutron density multiplied by track length in a volume and does not include neutron density multiplied by the average velocity unlike common presentation of neutron flux. Therefore, scaling factor may include the following conversion steps to get neutron flux at interested power level.

The fission rate can be estimated from the released energy per unit time and the power of the reactor. In order to produce power *P*, P/w_f fissions must occur per second (w_f is effective energy released per fission). This fission rate generates $P\bar{\nu}/w_f$ neutrons per second ($\bar{\nu}$ is average neutron released per fission).

To sum up, the scaling factor, *S*, may be calculated by using Equation 3.4.

$$S = \frac{P[W]\bar{\nu}\left[\frac{neutron}{fission}\right]}{\left(1.6022.10^{-13}\frac{J}{MeV}\right)w_f\left[\frac{MeV}{fission}\right]} \tag{3.4}$$

This approximation is appropriate for close to critical and steady state power level systems. Therefore, the multiplication effects for subcritical and supercritical systems ought to be included with $1/k_{eff}$. Consequently, actual total neutron flux can be shown as in Equation 3.5.

$$\phi\left[\frac{neutron}{cm^2 s}\right] = \frac{P[W]\bar{\nu}\left[\frac{neutron}{fission}\right]}{\left(1.6022.10^{-13}\frac{J}{MeV}\right)w_f\left[\frac{MeV}{fission}\right]}\frac{1}{k_{eff}}\phi_{F_4}\frac{1}{cm^2} \tag{3.5}$$

where ϕ_{F_4} is the flux from MCNP calculations of type 4 which represents flux averaged over a cell.

In addition, the reaction rate can be calculated by multiplying neutron flux and particular macroscopic cross section. In thermal power evaluation, the reaction rate shown in Equation 3.6 is extracted with tallies from MCNP output and used to derive heat generation at interested power level via scaling factor [29].

$$r_{MC} = \frac{1}{V}\int_V dV \int_{4\pi} d\Omega \int_0^\infty \phi_{MC}(r,\Omega,E)\sigma(E)dE \tag{3.6}$$

where r_{MC} describes the volume average reaction rate density which is normalized per source neutron and per target nucleus. The corresponding reaction rate *R* can be seen in Equation 3.7.

$$R = \int_V dV \int_{4\pi} \Omega \int_0^\infty \phi(r,\Omega,E)\Sigma(E)dE = \int_V dV \int_{4\pi} \Omega \int_0^\infty \phi(r,\Omega,E)N\sigma(E)dE \tag{3.7}$$

where *N* donates the number density of the interested nuclei. As a result, the relation between calculated and scaled reaction rates can be given as in Equation 3.8.

$$R = S \times N \times V_{fuel} \times r_{MC} \tag{3.8}$$

where V_{fuel} is the volume of interest. The generated power within the fuel can be calculated from energy dependent neutron flux as in Equation 3.9.

$$P = \int_V dV \int_4 d\Omega \int_0^\infty w_f(E)\sum_f(r,E)\phi(r,\Omega,E)dE \tag{3.9}$$

In MCNP calculations, Equation 3.9 can easily be simplified by assuming that *ν(E)* and $w_f(E)$ energy dependencies are negligible. Then, power generation can be calculated with Equation 3.10 for steady state and critical conditions.

$$P = R \times \nu \times w_f \tag{3.10}$$

where *R* scaled reaction rate here is specified as fission reaction rate.

3.2 Thermal Hydraulics

Thermal hydraulics is centered on fluid flow physics and energy (heat) transfer and the interaction between fluid and the surrounding structures. In nuclear engineering, thermal hydraulics includes more diverse dynamics than other industrial systems. It has a very wide range of subjects such as transfer of energy generated by fission to fluid and structures, gravity dominated flows in pipes, momentum driven critical flow through restrictions and passages, flow boiling and condensations, and lots of other phenomena.

This study aims to estimate the fuel and coolant temperature distributions, fluid velocity fields, form losses associated with pressure gradient along restrictions and passages on grid plates in ITU TRIGA Mark II core. In this regard, Navier-Stokes equation sets are solved numerically on fine gridded fluid domain with CFD

techniques. The main superiority of CFD techniques is that Navier-Stokes equations or simplified Reynolds Average Navier Stokes equations are solved by including the turbulent fluid flow. Therefore, it is possible to get a realistic and high accuracy solution in complex two or three-dimensional viscous flow.

3.2.1 Navier-Stokes Equations

The flow field of a Newtonian fluid can be fully described by the Navier-Stokes equations. The governing equations for fluid flow are conservation of mass, momentum, and energy equations. These partial differential equations are given in Equations 3.11 to 3.15 [30].

Conservation of Mass:

The continuity equation mathematically represents the rate of change of mass in a control volume equals to the mass flow rate into control volume minus the mass flow rate out of control volume. The continuity equation can be written in vector form as in Equation 3.11 below.

$$\frac{\partial \rho}{\partial t} + \nabla.(\rho \vec{v}) = 0 \tag{3.11}$$

Conservation of Momentum:

The momentum equation mathematically represents the rate the of change momentum in a control volume equals to the momentum flow rate into the control volume minus the momentum flow rate out of control volume plus net external force (for example; gravitational, electrical, and magnetic forces) including body forces and surface forces on control volume and given in vector form as in Equation 3.12.

$$\rho \frac{D\vec{v}}{Dt} = -\nabla p + \mu\left[\nabla^2.\vec{v}\right] + \rho \vec{f} \tag{3.12}$$

Conversation of Energy:

The energy equation mathematically represents the rate of change of internal energy in infinitesimal volume equals to the internal energy flow due to net mass flow on control volume plus heat transported diffusively and generated minus work performed by the medium in the volume and the work needed to put flow through the volume. The energy equation which is solved by FLUENT code can be written in vector form as in Equation 3.13 [31].

$$\frac{\partial}{\partial t}(\rho E) + \nabla.(\vec{v}(\rho E + p)) = \nabla.(k_{eff}\nabla T - \sum_j h_j \vec{J}_j + \bar{\bar{\tau}}_{eff}.\vec{v}) + S_h \qquad (3.13)$$

where k_{eff} is effective thermal conductivity (k_{eff} = k + k_t, where k_t is turbulent conductivity) and J_j is diffusion flux of species.

As it can be seen from conservation equations that they are second order nonlinear partial differential equations (PDEs). Even though they have limited analytical solutions for laminar and steady state flow, CFD tools provide amenable solutions for turbulent and laminar flows.

Although Navier-Stokes equations can describe turbulent flows in full detail, CFD tools for 3D complex geometries are not capable of solving turbulent flows in full detail due to their inherently unsteady flow pattern which involves large and extremely small eddies. They are computationally expensive to directly solve for very fine gridded domain in practical engineering calculations.

There are several methods to tackle turbulence in numerical analysis. Direct Numerical Simulation (DNS) offers to resolve all turbulence phenomena at all length scales and time steps while directly solving Navier-Stokes equations. It requires very fine meshing, time scaling, and advanced computational power. Another computational approach for turbulence modelling is Large Eddy Simulation (LES). This method solves spatially averaged, “filtered”, Navier-Stokes equations. While large eddies are directly solved, small eddies which are smaller than grid size are solved by isotropic eddies with some correlations. Although computational effort is less than DNS, it is still too expensive in time for most practical applications. Reynolds-Averaged-Navier-Stokes (RANS) model is the most commonly used approach for complex 3D flows. The advantage of this models is that it is less expensive in time than other approaches since this method solves time averaging Navier-Stokes equations. This approach has been used in this thesis. Therefore, turbulence modelling section is dedicated to RANS approach in Section 2.2.3.

3.2.2 Natural Convection

In ITU TRIGA research reactor, the heat generated from fission event is removed by natural convection. Natural convection, also known as buoyancy driven flow, is a phenomenon in which the fluid motion is caused by density differences due to temperature gradients when gravity or other proper accelerations act. Buoyancy flows

can be explained by Boussinesq approximation in fluid dynamics problems. In this regard, Boussinesq approximations assume that " variations in fluid properties other than density ρ are ignored and density only appears when it is multiplied by g the gravitational acceleration." [32]. Therefore, the contribution of buoyancy effects is shown on the momentum conservation equations rather than continuity or energy conservation equations. The momentum equation can be rearranged for natural convection as in the following equation derivations.

The general momentum equation for incompressible Newtonian fluids is shown in Equation 3.14.

$$\rho \frac{D\vec{u}}{Dt} = -\nabla p + \mu \nabla^2 \vec{u} + F \tag{3.14}$$

where F donates the sum of body forces. In the buoyancy driven flows, density has a linear dependence to temperature gradient as in Equation 3.15.

$$\rho = \rho_0 - \rho_0 \beta \nabla T \tag{3.15}$$

where the constant density ρ_0 is the density of the fluid at average temperature T_0 in working conditions. Thermal expansion coefficient β is slope of the linear function and it is also taken as approximate value due to unknown range of temperature.

If $F = \rho g$, according to Boussinesq equation, momentum conservation equation in vector form can be rewritten for natural convection as in Equation 3.16.

$$\rho_0 \frac{D\vec{u}}{Dt} = -\nabla (p - \rho_0 g\vec{k}) - \boxed{\rho_0 \beta \Delta T g\vec{k}} + \mu \nabla^2 \vec{u} \tag{3.16}$$

It is clear that momentum and energy equations are coupled since the temperature dependent density causes fluid flow. Therefore, they should be instantaneously solved.

In pure natural convection flows, the strength of buoyancy induced flow can be estimated by Rayleigh number. If the Rayleigh number is less than 10^8, natural convection flow indicates laminar flow; otherwise, transition and turbulence flow regime occur over the range of $10^8 <$ Ra $< 10^{10}$.

In this thesis, in order to determine the flow regime, Rayleigh number is estimated as 6.45×10^{11} by assuming ΔT is 40 °C, the characteristic length of surface is 1 m and fluid properties are taken at 25 °C. As a result, the Ra number shows that the flow regime in TRIGA core is fully turbulent.

3.2.3 RANS Turbulence modelling

In the scope of this thesis, RANS model is employed to simulate turbulent flow regime. In a turbulent flow, velocity and pressure of fluid flow may include a mean part and a fluctuating part. In order to treat the decompositions of the variables as mean and fluctuating part, RANS model manipulates N-S equations by averaging time or ensemble. By reducing the resolution of small eddy quantities, the modified set of equations can be solved within reasonable computational costs.

In the Reynolds averaging, the solution variables can be decomposed into the mean part and fluctuating parts. The velocity components are shown in Equation 3.17.

$$u_i = \bar{u}_i + u_i' \tag{3.17}$$

where, $\bar{u}_i$ and u_i' represents mean and fluctuating components (*i=1,2,3*). In the same way, other scalar quantities can be generalized as in Equation 3.18.

$$\Phi = \bar{\Phi} + \Phi' \tag{3.18}$$

where Φ donates a scalar quantity such as pressure, species or energy.

The continuity and momentum equations are arranged by substituting the expressions as the form in Equation 3.18 for variables, taking time or ensemble average, and dropping the overbar on the mean velocity. The arranged equations give Reynolds averaged Navier-Stokes equations in cartesian tensor form as in Equation 3.19 and 3.20.

$$\frac{\partial \rho}{\partial t} + \frac{\partial}{\partial x_i}(\rho u_i) = 0 \tag{3.19}$$

$$\frac{\partial}{\partial t}(\rho u_i) + \frac{\partial}{\partial x_j}(\rho u_i u_j) = -\frac{\partial p}{\partial x_i} + \frac{\partial}{\partial x_j}\left[\mu\left(\frac{\partial u_i}{\partial x_j} + \frac{\partial u_j}{\partial x_i} - \delta_{ij}\frac{\partial u_l}{\partial x_l}\right)\right] + \frac{\partial}{\partial x_j}(-\rho\overline{u_i' u_j'}) \tag{3.20}$$

They are same in form with instantaneous N-S equations, but now one additional term appears which demonstrates the effects of turbulence. Here, $-\rho\overline{u_i' u_j'}$ is called Reynolds Stress and must be modeled. Boussinesq hypothesis is used commonly to relate Reynolds stresses to mean velocity vectors as in Equation 3.21 [33].

$$-\rho\overline{u_i' u_j'} = \mu_t\left(\frac{\partial u_i}{\partial x_j} + \frac{\partial u_j}{\partial x_i}\right) - \frac{2}{3}\left(\rho k + \mu_t \frac{\partial u_k}{\partial x_k}\right)\delta_{ij} \tag{3.21}$$

where μ_t represents turbulent kinematic viscosity.

RANS based closure models *k-ε* and *k-ω*, and *SST* hybrid models have different approaches for turbulent kinematic viscosity, production, and decay. RANS based *k-ε* closure model is employed within this thesis. In the case of *k-ε* model, it includes two additional transport equations (one for turbulence kinetic energy *k* and the other for turbulent dissipation rate *ε*) and turbulent kinematic viscosity μ_t is calculated as a function of *k* and *ε* with a relation as shown in Equation 3.22.

$$\mu_t \propto \frac{k^2}{\varepsilon} \tag{3.22}$$

In this thesis, turbulence modelling phenomenon is not the main point of interest. However, Sal Rodriguez has explained the fundamentals of RANS turbulence modelling with deeper understanding of turbulence phenomena [34]. Furthermore, a comparative study on turbulence models in CFD codes is achieved in the University of Ljubljana with illustrative turbulence models [35].

3.2.4 Conjugate heat transfer model

In the TRIGA core model, the second part of CFD modelling which is described in Section 4.3.2, conjugate heat transfer method is used to predict thermal-hydraulic core parameters in detail. In this method, numerical analysis involves heat transfer solution in both solids and fluids therefore heat transfer along the fuel rod is performed by solving heat conduction equations whereas the transport of energy in fluid is performed by energy equations with convective contribution.

The TRIGA fuel rod has four regions radially: central zirconium rod, $UZrH_{1.65}$ fuel meat, hydrogen filled gap, and stainless steel clad as seen in Figure 3.2. In this regard, the heat generated by fission transfers radially out of the fuel meat first reaches to the gap and then to the clad and finally the coolant.

The heat conduction equations for a typical cylindrical fuel element (Figure 3.3) can be developed by using below derivations. In the figure, *r* represents the radius of a region defined with subscript *f* for fuel meat, *g* for gap, and *c* for clad. Similarly, temperatures at the edge of each region are given with the same subscripts.

1. Heat conduction with a uniform volumetric heat source q''' :

The conduction equation for the fuel meat is given by Equation 3.23.

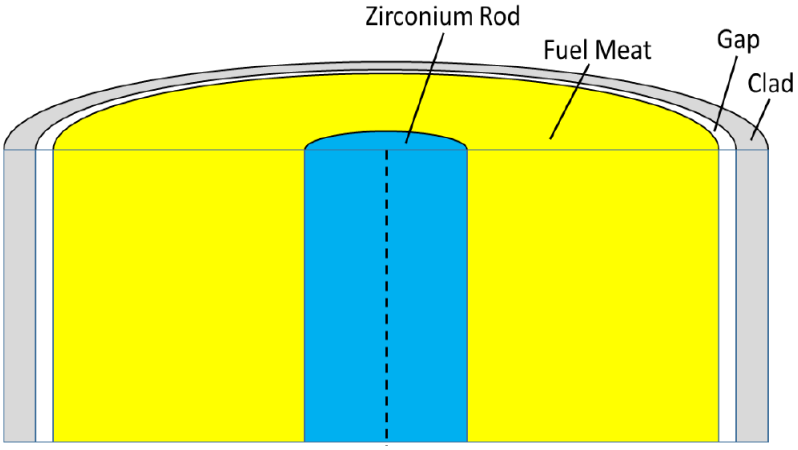

Figure 3.2 : TRIGA fuel element radial components considered for conduction calculations [36].

$$\frac{1}{r}\frac{d}{dr}\left(k_f r \frac{dT}{dr}\right) = q''' \tag{3.23}$$

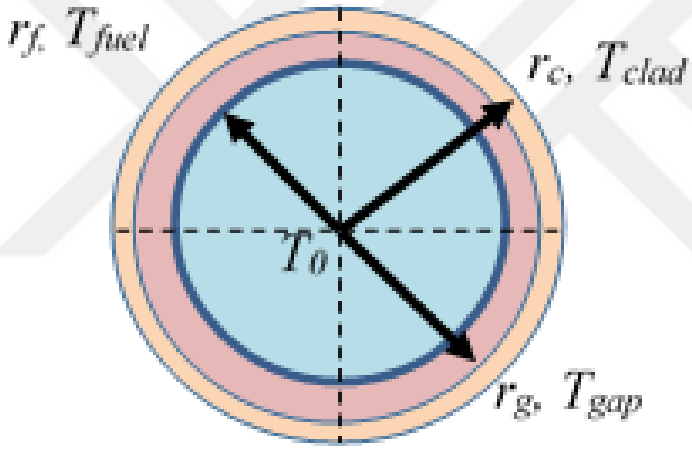

Figure 3.3 : The geometry of a typical cylindrical fuel rod.

Integrating Equation 3.23 with assuming constant fuel conductivity k_f and applying boundary conditions of $\left.\frac{\partial T}{\partial r}\right|_{rf=0} = 0$ and T=T0 at $r = 0$ will yield temperature difference between the fuel surface and rod centerline (Equation 3.24).

$$\Delta T\big|_{FUEL} = T_0 - T_f = \frac{r_f^2}{4k_f} q''' \tag{3.24}$$

2. Heat conduction without heat source:

Since there is no heat generation in the gap and the clad, Equation 3.23 takes the form of Equation 3.25.

$$\frac{1}{r}\frac{d}{dr}\left(kr\frac{dT}{dr}\right)=0 \tag{3.25}$$

For the gap region of thickness t_{gap}, integration of Equation 3.25 with assuming constant gap conductivity k_{gap} and applying boundary condition $T = T_{gap}$ at $r = r_{gap}$ (where $r_{gap} = r_f + t_{gap}$), the temperature difference between the fuel surface and gap outer surface is shown in Equation 3.26.

$$\Delta T\big|_{gap} = T_g - T_f = \frac{q''' r_f^2}{2k_g} In\left(\frac{r_g}{r_f}\right) \tag{3.26}$$

With the assumption of very small gap thickness, Equation 3.26 can be rearranged as in Equation 3.27.

$$\Delta T\big|_{gap} = T_g - T_f = \frac{q''' r_f}{2}\left(\frac{t_g}{k_g}\right) \tag{3.27}$$

The same methodology can be applied to the clad region because this region does not have heat generation, either. Assuming that clad conductivity k_{clad} is constant and $T = T_{clad}$ at $r = r_{clad}$ ($r_c = r_f + t_g + t_c$ where t_c is clad thickness), the temperature difference between the gap and clad surface can be found with the Equation 3.28.

$$\Delta T\big|_{clad} = T_c - T_g = \frac{q''' r_f}{2}\left(\frac{t_c}{k_c}\right) \tag{3.28}$$

3.2.5 Computational Fluid Dynamics Code: FLUENT

In thermal-hydraulic analysis, the CFD code FLUENT in the commercially packaged ANSYS workbench is used [37]. FLUENT code has the capability to simulate fluid flow as well as heat transfer across solid and fluid domains and solid to solid heat flow. It solves the discretized governing equations using finite volume approach for steady and time dependent problems. FLUENT code provides comprehensive numerical solution on different media such as liquid, gaseous, porous, and solid media. Furthermore, it includes heat transfer models, such as conduction, radiation, and convection.

A typical CFD simulation can be created with four steps: geometry modeling, mesh generation, physical model set up, and post-processing of the computed data. In this thesis, preprocessing (geometry modeling and mesh generation) is performed by the ANSYS package “design and mesh module” [38].

Setting up the solver is a critical step to create an efficient CFD model in terms of convenient physics representation. Regarding to solution algorithms, FLUENT has two main solver technologies to solve continuity, momentum, if included energy and species equations: the density based and pressure-based solvers that have different way for the solution of these equations. In this thesis, the pressure-based solver is used since it is developed for low speed incompressible flows.

According to FLUENT theory guide, pressure-based algorithm based on the pressure equation that is derived by rearranging the continuity and the momentum equations in a way that the velocity field, obtained by solution of pressure equation or pressure correction, allows the update of continuity equation [39]. To achieve a solution, the governing equations are solved iteratively, since the governing equations are nonlinear and coupled. The pressure-based solver has two approaches to solve flow problems: segregated and coupled algorithms. The algorithm loops can be represented as in Figure 3.4 for both manners.

The segregated loops contain solution variables (*u, v, w, p, k,* and ε etc.*)* that are obtained by solving individual governing equations one after another; that is, each equation is solved either in "decoupled" or segregated from. Since the discretized equations are stored in the memory once at a time, this algorithm needs less memory size than the coupled algorithm, but convergence is slow in comparison with the coupled solver.

The pressure based coupled algorithm includes a coupled system of equations including momentum and pressure-based continuity equation. Thus, unlike segregated algorithm, solving momentum equation by updated values of pressure and face mass flux and then pressure correction with new velocity field and mass flux steps are combined by one single step. As a result, the rate of solution convergence becomes significantly better than the segregated algorithm. However, it needs 1.5 - 2 times memory size than segregated algorithm does.

Another crucial aspect of CFD modelling is the determination of appropriate boundary conditions for the flow of interest. The flow and thermal properties on the boundaries must be given by boundary condition specifications. FLUENT classifies boundary types as flow inlet and exit boundaries, wall, repeating, and pole boundaries, internal cell zones, and internal face boundaries.

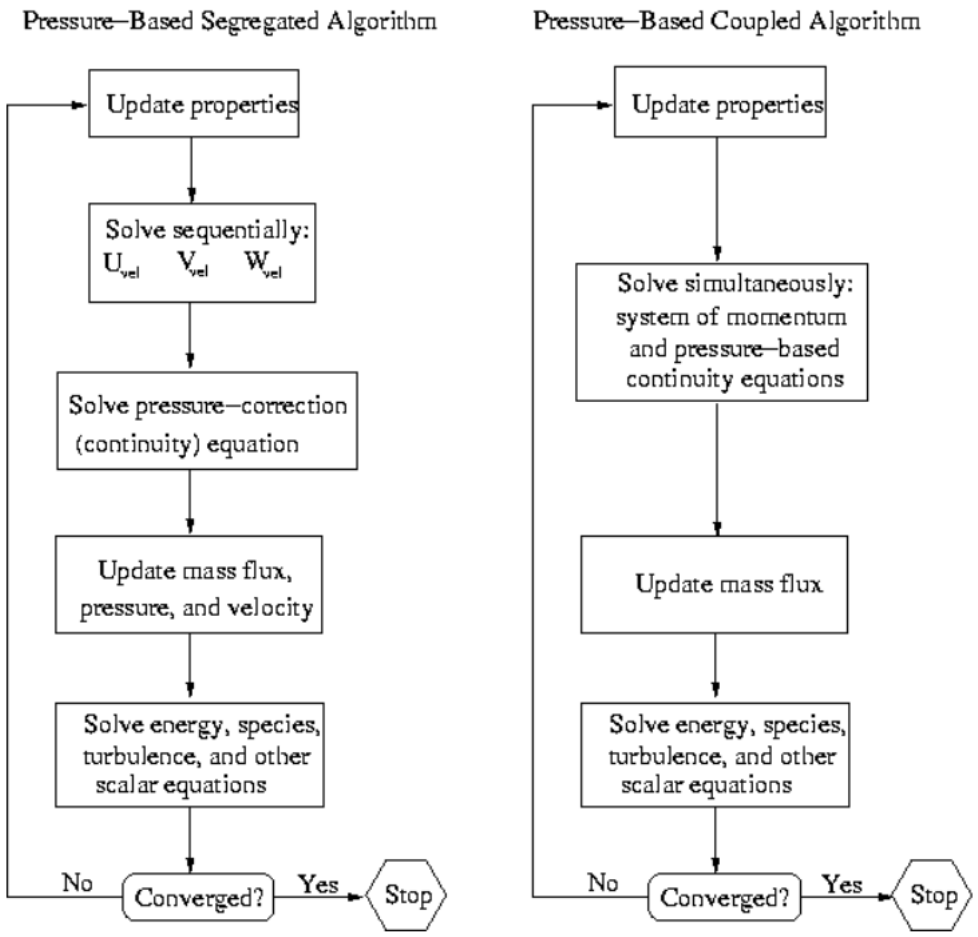

Figure 3.4 : The algorithm of pressure based segregated and coupled solvers [40].

Considering the modelling in specified flows, the standard features of FLUENT code may not have the capability to represent realistic flow physics. To overcome this problem, FLUENT code allows the implementation of special needs with User Defined Function (UDF) which is a small program written in C programming language. UDF files can be used to customize boundary conditions, material property definitions, source terms in transport equations as well as the initialization of solution, time dependent adjustment of variables such as velocity, pressure etc. There are basic features and needs to build a UDF file. To encode a UDF, "udf.h" library must be included and DEFINE macros supplied by FLUENT to access the solver must be used [41]. The variables can be defined on computational grid components such as face, cell, node, and edge.

In pool modelling performed in this thesis, in order to specify cosine shape heat flux boundary conditions along the z axis of active region (the region where fission occurs) on clad surface, DEFINE_PROFILE macro is used. In core modelling, the volumetric

heat source in cosine shape in the fuel region is given using DEFINE_SOURCE macro and temperature dependent material properties specified by DEFINE_PROPERTY macros on cell data [42]. The examples of generated UDFs for the heat flux and temperature dependent material property are included in Appendix A.

4. METHODOLOGY, RESULTS AND DISCUSSIONS

4.1 ITU TRIGA Mark II Research Reactor Description

ITU TRIGA Mark II research reactor is 250 kW open pool type research reactor. It can pulse up to 1200 MW for short periods of time. The reactor core is submerged in a 2 m diameter Aluminum tank filled with deionized light water as seen in Figure 4.1 which provides approximately 5 meters water head above the core at nearly 151 kPa. The water acts as coolant, moderator, and shield. The bulk pool temperature at shutdown state and operating state depends on season. According to operation log-book, the average pool temperature is 25 °C in summer and 20 °C in winter.

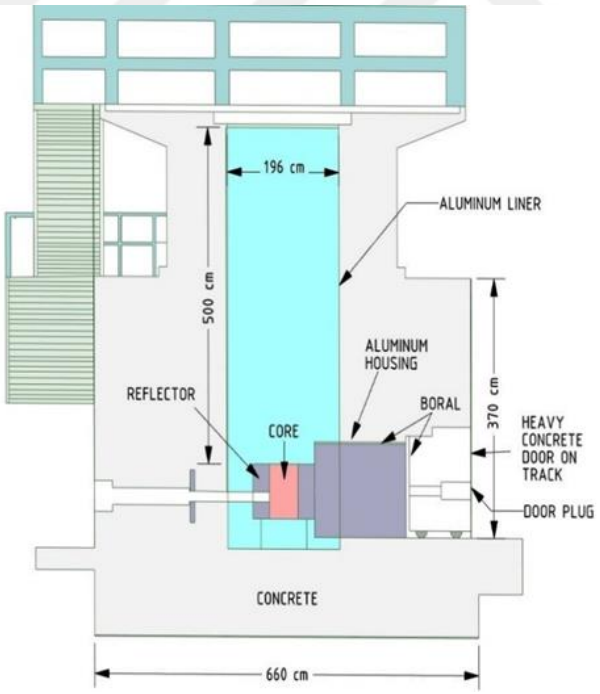

Figure 4.1 : ITU TRIGA Mark II research reactor side view.

The primary method of cooling is natural convection; furthermore, the mixed convection (forced + natural) is provided by the primary cooling system to maintain average pool temperature below 40 °C for any operation. The primary cooling system comprises a pump, a heat exchanger, associated valves and piping, ^{16}N diffuser, and temperature probes [9].

The TRIGA reactor core is surrounded by graphite reflector and consists of six concentric rings; A, B, C, D, E, and F and each of them has 1, 6, 12, 18, 24, and 30 locations, respectively for fuel-moderator elements, control rods, graphite dummy elements, source element, pneumatic transfer system, and in-core experimental devices such as the central thimble (Figure 4.2). In this regard, core components and design parameters are given in Table 4.1 [43]. All these elements are accurately spaced and supported by aluminum top and bottom grid plates. The top grid plate has 3.8227 cm holes to allow insertion and withdrawal of fuel-moderator elements. In addition, the top grid plate has 16 foil insertion holes with 0.8227 cm diameter for measurements of core temperature and/or neutron flux [44]. The reactor is controlled by three control rods made out of boron carbide (B_4C), a neutron absorber material, encapsulated in aluminum cladding. These are called regulating, safety, and transient control rods and placed in different rings in the core to guarantee the safe shutdown of the reactor. The core-out irradiation utilities are comprised of three beam tubes (piercing, radial, and tangential) that are pierce into the biological concrete shield surrounding the aluminum tank. There is also a thermal column.

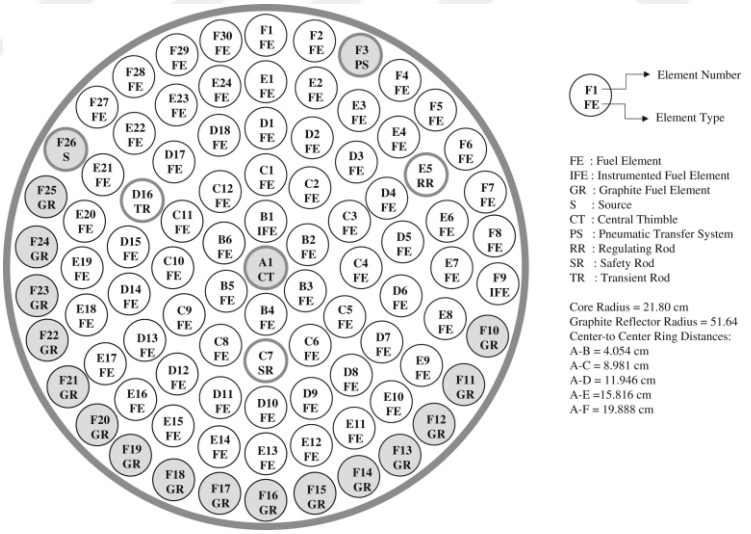

Figure 4.2 : ITU TRIGA Mark II core configuration [7].

The TRIGA fuels, developed by General Atomics, were designed around the concept of inherent safety. The fuel consists of a homogeneous mixture of uranium, containing 8.45% U enriched no more than 20% ^{235}U, and Zirconium Hydride $ZrH_{1.65}$, (where 1.65 is the ratio of Hydrogen to Zircon atoms.). The superiority of this type of fuel element is that it behaves as fuel and moderator. In this regard, Hydrogen acts as a moderator, whereas Zirconium acts as “sponge” for the absorption of Hydrogen to

create convenient hydrogenous medium. To achieve this, the center of fuel meat is drilled with a 0.635 cm diameter hole and a Zirconium rod is plugged after the center hole hydration is completed [12]. Cylindrical Graphite plugs are placed above and below of active region where fission events happening of fuel element; thus, the core is also reflected axially.

Table 4.1 : The general description of ITU TRIGA Mark II research reactor [43].

Reactor Type	TRIGA Mark II	
Maximum steady state power level	250 kW	
Maximum pulse power	1200 MW	
Fuel Element Design	Fuel meat material	$UZrH_{1.65}$
	Uranium content	8.5 wt %
	Uranium enrichment	20 % ^{235}U
	Cladding material	Type 304 stainless steel
	Active fuel height	38.1 cm
	Fuel element outer diameter	3.75412 cm
	Clad thickness	0.0508 cm
	Gap thickness	0.00381 cm
	Zircon rod diameter	0.5715 cm
Number of fuel elements	69	
Number of reflector elements	16	
Reactor cooling	Natural Convection	
Number of Control Rods	Safety	1
	Regulating	1
	Transient	1
In core experimental devices	Central thimble	1
	Pneumatic system	1

The reactor stability is generally governed by reactivity feedbacks. Therefore, reactor design must provide that the temperature feedbacks are negative under all operating conditions. In this regard, $UZrH_{1.6}$ mixed fuel ensures a large prompt negative temperature reactivity coefficient that has “completely” and “inherently” safe emphasis on TRIGA reactor for reactivity insertion events.

The inherently safe concept can be explained by three mechanisms based on fuel temperature rise [45]. The first and second mechanisms relate to the possibility of a thermal neutron to gain energy from excited state of an oscillating hydrogen atom in the lattice as the hydride temperature increases. Since the neutron gains energy,

average neutron energy shifts upward, and this phenomenon is known as spectrum hardening. The first spectrum hardening effect on reactivity depends on the probability of neutron leakage from fuel elements before neutron being captured in the fuel. Therefore, the percentage of absorption in fuel decreases as the neutron leaks to water. In this way, the core neutron balance tends to lose reactivity. This phenomenon is known as “cell and non-homogenous effect” and is an important contribution of prompt negative coefficient. The second effect of spectrum hardening is the core leakage contribution on prompt negative coefficient. It has basically the same the mechanism as the cell effect. In this regard, the core can be considered as a large super cell with the graphite reflector acting as the moderator. The leakage from the core is increased as the core heats up and capture event comes off outside of the fuel. In this way, the negative reactivity insertion is occurred in the core. The third contribution on prompt negative reactivity is Doppler broadening effect. The ^{238}U capture resonance region is broadened by the rising temperature of fuel. Consequently, the resonance escape probability is reduced and the more capture in ^{238}U occurs thereby, the reactor stability is provided by decreasing neutron population.

According to General Atomics experiments at Brookhaven Laboratory, integrated mixed UZrH fuel ensures not only aforementioned basic neutron spectrum hardening mechanism to satisfy inherently safe reactor but also good heat capacity, low chemical reactivity with water, excellent fission retention, and reasonable low hydrogen pressure equilibrium pressures at high temperatures [46].

4.2 Neutronic Modelling

In the scope of this thesis, ITU TRIGA Mark II research reactor neutronic model created with MCNP 6.2 code by Asst. Prof. Dr. Senem Şentürk Lüle is modified to determine neutron flux distribution throughout each fuel element to calculate the heat generation in each fuel element. In other words, output of neutronic calculations became the input of thermal hydraulics calculations. This neutronic model was developed with detailed specifications about geometry, material, and nuclear data to avoid modelling and systematic errors as much as possible. In this regard, the model included well-defined fuel elements, control rods, in core experimental tools, graphite reflector, in-core irradiation ports, rotary specimen rock groove, the beam ports, and surrounding concrete biological shielding. The neutronic calculations were performed

with ENDF/B-VII data libraries for continuous energy interactions and $S(\alpha,\beta)$ kernel scattering tables to treat low energy (< 4 eV) thermal scattering contribution for ZrH and H_2O moderation materials.

In the thesis, the source term was given by KCODE (criticality problem) card and KSRC card (initial spatial distribution of fission points). In this respect, 1700 cycles, 1500 of which being active cycles, with 25000 neutrons per cycle were used. Therefore, the number of neutrons sampled is totaling 3 million and keeping standard deviation of the results to 0.0001 level.

The neutronic model had to be validated before being used in thermal hydraulic study to provide appropriate parameters. Therefore, the results of another study at Energy Institute that employs the same MCNP input deck was taken into account. In that study, neutronic analysis was performed, assuming cold zero power operating conditions at 25 °C without any burn-up effect. Namely, the fuel elements had been considered to be fresh without Xenon. Consequently, the results had been benchmarked against worth of control rods and effective delayed neutron fraction from experimental data. As seen Table 4.2, the worth of control rods are in good agreement with experimental data as well as the effective delayed neutron fraction β_{eff}.

Table 4.2 : Benchmarking neutronic MCNP model with experimental data.

Control Rod Worth	MCNP	Experimental	% Error
Transient ($)	3.08	3.16	2.5
Safety ($)	2.19	2.18	0.5
Regulating ($)	1.84	1.84	0.0
β_{eff}	0.00721	0.0073	1.2

In order to perform thermal hydraulic simulations, the axial distribution of volumetric heat generation in each fuel element was required. The power level of the fresh core was adjusted to 250 kW with all control rods are fully out of the core. In this regard, cell averaged flux (F4) and superimposed mesh tally (FMESH) features of MCNP code were employed [46]. The FMESH tally artificially divided active fuel length of 38.1 cm into 19 cells with a length of approximately 2 cm in axial direction as seen in Figure 4.3.

In order to get power distribution within newly generated artificial cells superimposed on the active fuel region of each fuel element, F4 tally was employed with the FM

multiplier card. F4 tally gives average neutron fluence over a cell; however, the power density calculation needs the fission reaction rate with the scaling factor as stated in Section 3.1.3.2. Therefore, the integral term of Equation 3.1 is extracted by using F4 tally with "-6" as multiplier option to acquire "$\nu\sigma_f\phi_{F4}$" term.

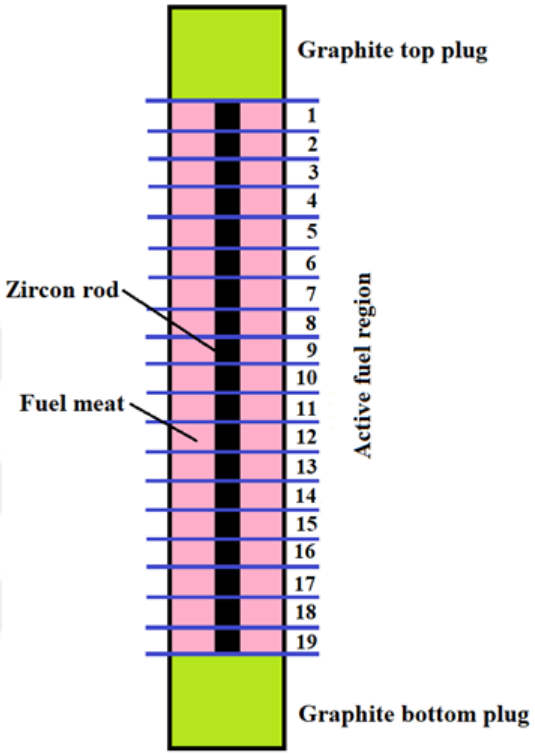

Figure 4.3 : Axial meshing of active fuel region for volumetric heat generation calculation.

$$p(r) = \frac{PM}{\not{w}_f}\not{w}_f N\nu\sigma_f\phi_{F4} \rightarrow r \in {}_{\Delta}V_i \tag{4.1}$$

where σ_f represents the microscopic fission cross section.

In order to take material composition of fuel element into account, macroscopic cross section is required. Therefore, the integral should be multiplied by the atom density of sampled material (UZrH). The negative sign in multiplier card in front of option "6" mentioned above automatically calculate the atomic density of sampled material in scaling factor term therefore vanishes the need for hand calculation.

The Monte Carlo simulations were performed on high power computing system at the ITU Energy Institute bought through a project of Asst. Prof. Dr. Senem Şentürk Lüle which is supported by ITU Scientific Research Project Unit. The computations took approximately 30 minutes when 40 processors were used in parallel computing.

Figure 4.4 shows the power generated by each fuel element as a result of 250 kW operation of the reactor. The maximum power per element is around 5500 W.

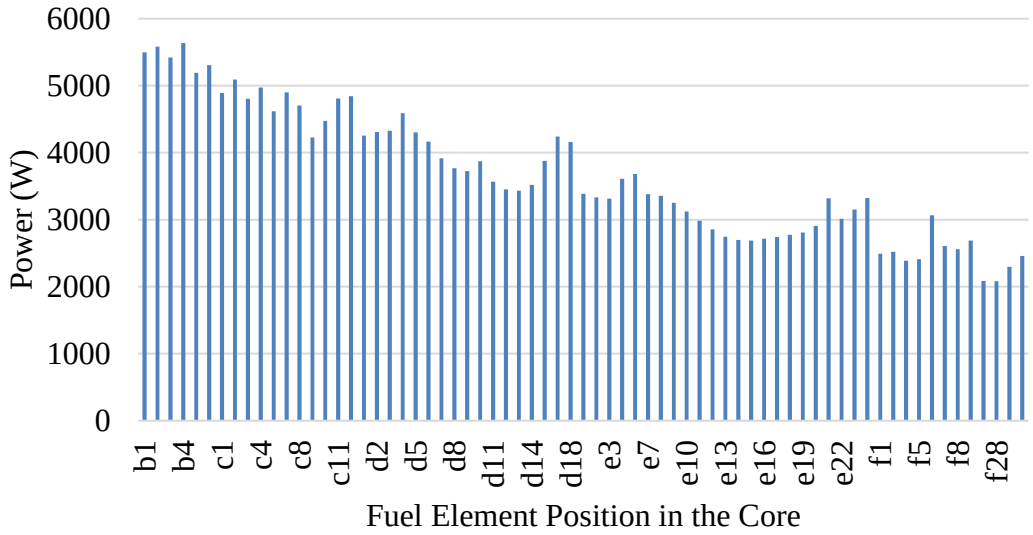

Figure 4.4 : Power generated by each fuel element for 250 kW nominal power.

These results that are from simulations using F4 tally with FM card and FMESH superimposed mesh tally were verified with the results of another study performed at the Energy Institute involving burnup calculations in which fuel elements were considered as one body. The normalized power distribution seen in Figure 4.5 indicates that the power production throughout the core peaks around the core center, as more enriched fuel elements are located there. Therefore, the hottest channel and hottest fuel elements would be around this area.

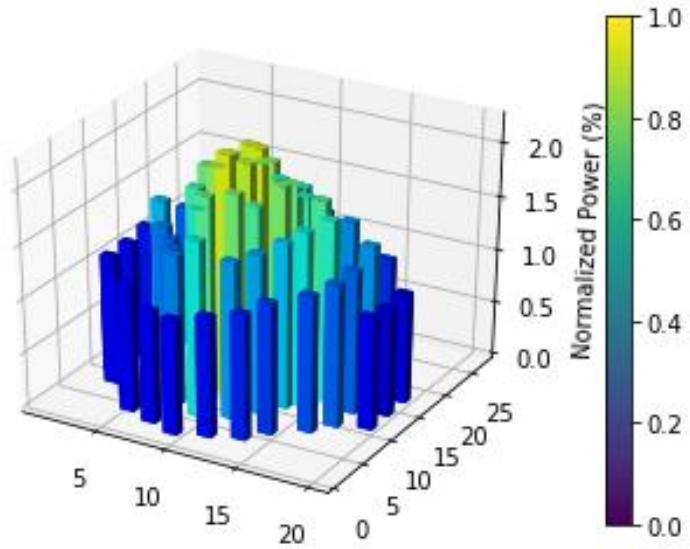

Figure 4.5 : ITU TRIGA Mark II core power distribution.

Furthermore, the average, maximum and minimum power per fuel element, ratios of maximum-to-average power and maximum-to-minimum power are presented in Table 4.3. The Safety Analysis Report of TRIGA research reactor should include these calculated values.

Table 4.3 : Calculated average, maximum, and minimum power per fuel element.

Average power per fuel element (kW/element)	Maximum power per fuel element (kW/element)	Minimum power per fuel element (kW/element)	$\frac{P_{max}}{P_{avg}}$	$\frac{P_{max}}{P_{min}}$
3.67	5.64	2.08	1.54	2.71

In order to perform thermal hydraulic calculations to calculate axial temperature distribution in fuel and coolant, power production in each cell element must be defined in CFD code FLUENT. The axial distribution of power generation in each fuel element shows sinusoidal profile as seen in Figure 4.6.

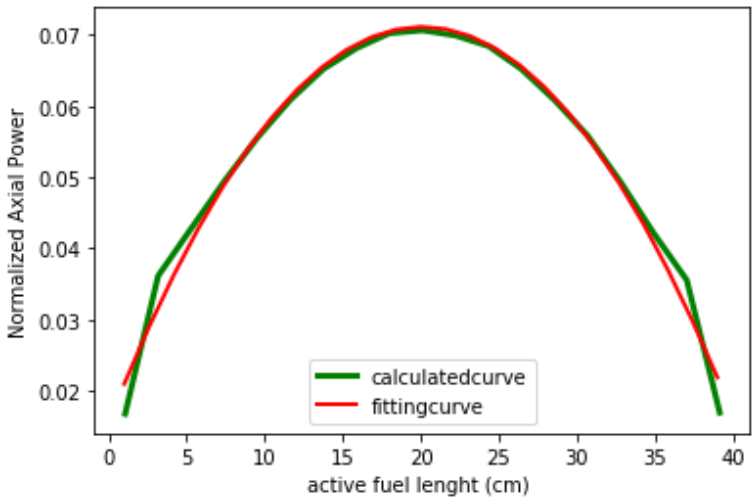

Figure 4.6 : Axial normalized power distribution along the active fuel region.

A second order polynomial curve fitting was performed to acquire the axial variation of volumetric heat generation in each fuel element and heat flux at the surface of each fuel element. The resulting general function is expressed in Equation 4.2. 69 such functions were then inserted as the thermal boundary condition by using UDF feature of FLUENT. A sample UDF out of 69 can be seen in Appendix A.

$$q'' = C(\ -1.3767z^2 + \ 2.6925z\ -\ 1.2454) \qquad (4.2)$$

where C is the total heat flux streaming from fuel clad that changes for each fuel element although axial behavior remains the same.

4.3 Thermal Hydraulic Modelling

The main scope of this thesis is to provide highly accurate 3D solution for neutronics and thermal hydraulic phenomena in ITU TRIGA Mark II research reactor. Since the governing physics of these phenomena are coupled, two solution models based on the governing physics principle should be performed integrally. In this way, the nuclear data and core parameters such as material temperatures especially the fuel temperature and coolant density were calculated as precisely as possible thanks to 3D conjugate heat transfer modelling.

In order to establish thermal hydraulic model of reactor, the detailed geometry that includes pool and core structures such as control rods and grid plates has to be included to simulate fluid dynamics/heat transfer. Unfortunately, the current computational resource is not sufficient for such a detailed modelling. Therefore, the thermal hydraulic investigation has been performed in two separated stages to reduce the computational cost. In this methodology:

At first stage, the TRIGA pool was modelled by FLUENT code to discuss natural convection circulation under steady-state full power condition to predict velocity field and pressure distribution in the core which will be used in the following stage. This stage is called as “the pool model” and will be discussed in Section 4.3.1.

At second stage, after completion of stage 1, only inside of the reflector was modelled to perform conjugate heat transfer. Therefore, this stage is called as “the core model”. In this model, heat conduction in fuel elements and natural convection were performed by FLUENT code. The details are given in Section 4.3.2.

The results of thermal hydraulic analysis were compared with experimental data of [12]. The validated calculated data such as the temperature of fuel elements and the coolant density and temperature were then used to upgrade the neutronic model.

4.3.1 TRIGA pool model

The objective of pool model is to simulate thermal hydraulic characteristics through the pool with CFD simulations. These characteristics include natural convection flow behavior, the pressure and velocity variation throughout restrictions and passages, the temperature distribution along the pool.

The CFD modelling was performed through following three primary steps that are required for any computational analysis. In this context, the so-called pre-processing step involves determination of computational domain and discretization of delineated geometry. In this thesis, the computation domain was constructed without any major simplifications. In this regard, the top and bottom grid plates (Figure 4.7) which create major flow restrictions in TRIGA RR were included in the pool model as accurately as possible. The structures in the core included in the pool model are

- Fuel rods with simplified end fittings,
- In-core irradiation channels,
- Graphite dummies,
- Control rods,
- Top and bottom grid plates,
- Thermal column,
- Graphite reflector.

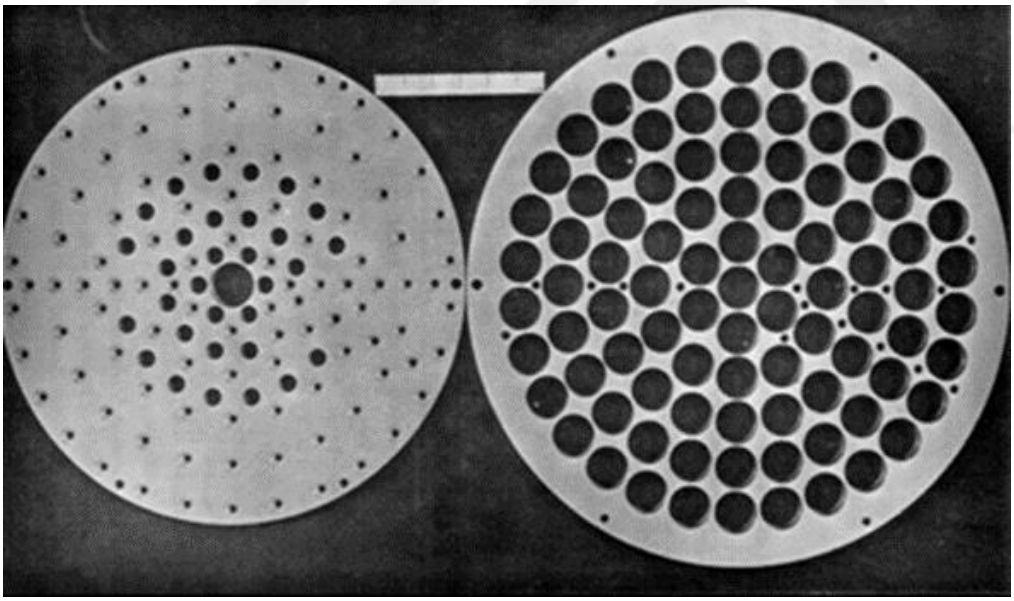

Figure 4.7 : Bottom (left) and top (right) grid plates.

The Figure 4.8 provides a clear understanding of the computational domain of CFD pool model. Finally, the pool model configuration was completed with unstructured mesh of maximum 5 cm face size totaling nearly 10 million grid points.

Thereafter, the differential equations governed by the natural convection phenomena were discretized into the algebraic equations by finite volume discretization method.

Furthermore, discretization was accomplished by unstructured meshing technique. The reason for using unstructured meshing is that it is suitable for discretizing complex geometries and has the capability of adaptive meshing techniques with faster meshing time [48]. Although additional CPU and memory are necessary in comparison to block structured or overset grid techniques, the unstructured mesh is well suitable for large scale parallelization due to its homogeneous data structure that provides ideal load balancing on a large number of processors [49].

The following step after pre-processing step is to set up an appropriate physical model. In this regard, the effects of natural convection were evaluated by considering buoyancy term $F = \rho g$ in momentum conservation equation. (Equation 3.14). Here, the dependence of fluid density on temperature can be addressed through the following two approaches.

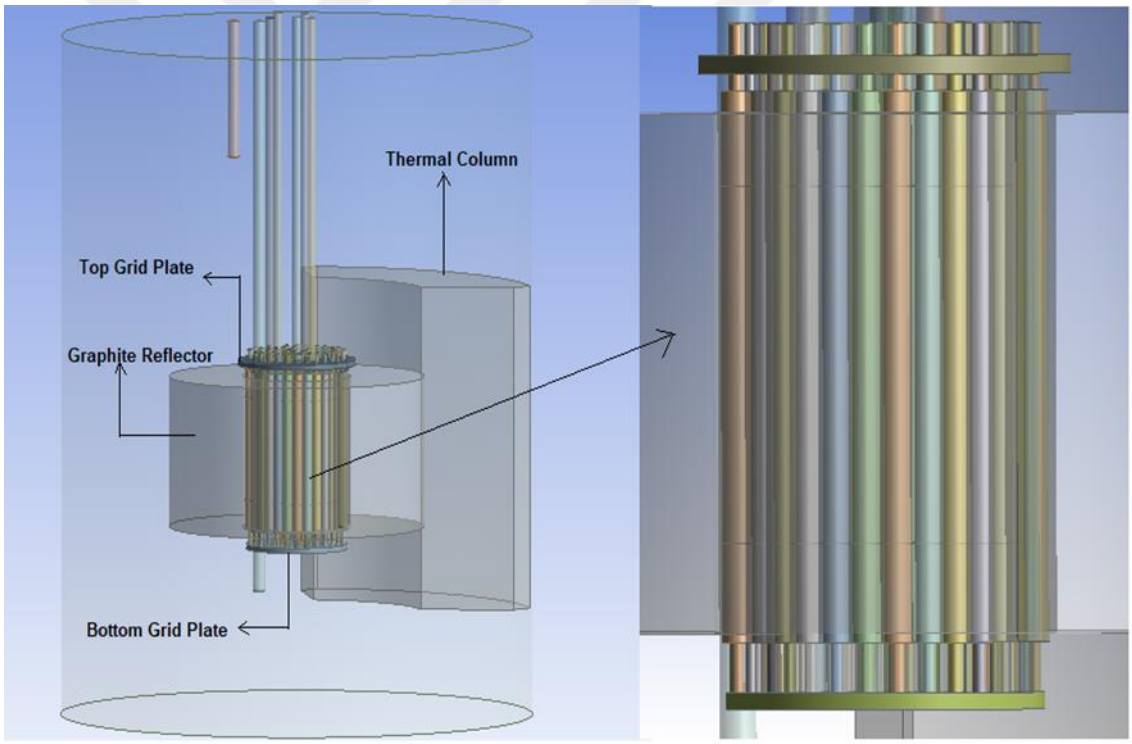

Figure 4.8 : The pool model geometry used for simulations.

The Boussinesq approximation described in Section 3.2.2 [50]. In this approach, the fluid density ρ is considered as a linear function of temperature (Equation 3.15). This approach is suitable if the temperature differences in the domain are quite small [50].

The fluid density is considered as a function of temperature. In unsteady nature flows such as natural convection, this approach should be used for better accuracy if temperature gradient is high [51].

In the CFD modelling, natural convection flow was modeled by using the second approach since the temperature variation in core is reasonably high. In this regard, the density of the coolant was interpreted as a polynomial function of temperature as well as specific heat capacity [52]. The polynomial density and specific heat functions was determined by fitted data from Table A.1 [53]. The transient solution was accomplished; as natural convection flow is inherently unsteady. In addition, the turbulence effects were considered by unsteady RANS approach with k-ϵ closure models defined in Section 3.2.3.

In the pool model, it was assumed that the convection flow occurs only in the stationary water. On the other hand, zero velocity and gauge pressure was assigned to inlet and outlet of fluid domain. Moreover, the thermal boundary conditions on surface of fuel elements were given with heat-flux boundary conditions. In this regard, the axial cosine shape of heat flux as stated in Section 4.2 was adjusted on the fuel surface via UDF feature of FLUENT. Finally, no-slip conditions were applied to all surfaces. Other set- up procedures applied to the FLUENT code are briefly given in Table 4.4.

Table 4.4 : Numerical set up of FLUENT code for pool model.

Feature	Applied method	Definition
Numerical method	Finite volume	
Solver	Pressure based solver	
Solver algorithm	Segregated approach	SIMPLEC
Turbulence model	RANS	Realizable k-ϵ model
Pressure interpolation scheme (including the momentum equations)	Natural Convection Dominated flow	Enhanced wall treatment PRESTO (Pressure Staggering Option)
Spatial discretization	Convection terms (except for pressure term in the momentum equations)	Second order Discretization
Time discretization		0.005
Convergence criteria	Relative or Absolute	

The CFD modelling was performed assuming that the reactor is at 250 kW full power, in steady state operation and operating bulk temperature is 25 °C. The URANS simulation is performed till flow reach steady state.

CFD simulations were performed on high power computing system at the ITU Energy Institute. The computations took approximately 8 days when 28 processors were used in parallel computing.

To determine whether the natural circulation has reached a steady state, monitoring of the solution data had been carried out. In this context, thermal-hydraulic parameters such as wall temperature, coolant density, and velocity were investigated at a certain point in the pool. Depending on the thermal-hydraulic parameter fluctuations in time, natural convection flow reached a steady state within 50 seconds in seen in Figure 4.9

The result showed that the maximum temperature in core is around B4 fuel element. Since the natural convection heat transfer has not yet dominated the heat transfer mechanism, the temperature has rapidly increases in a few seconds as seen in Figure 4.9. In addition, the heat convection transfer mechanism takes dynamic form that will allow sufficient cooling of fuel elements after the simulation time of 10 seconds.

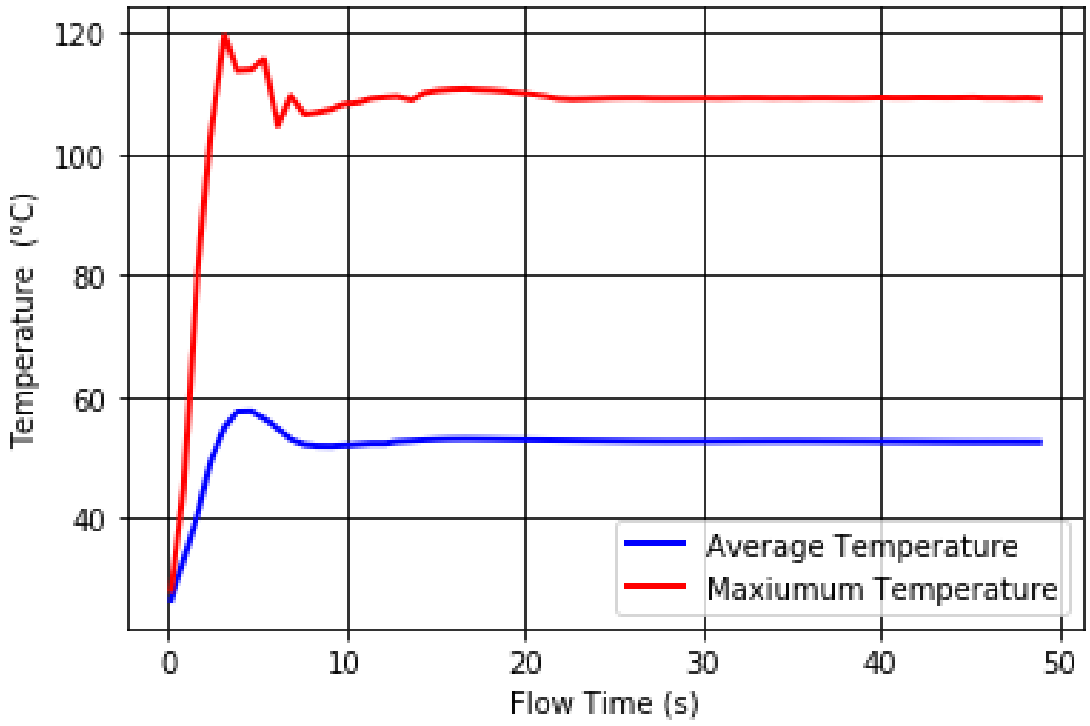

Figure 4.9 : The time dependence of temperature around B4 fuel element.

To provide a better understanding of relationships between flow parameters based on natural convection phenomenon, velocity and density of the coolant were obtained at a reference point that is located between B1 and C1 fuel elements.

In this regard, the density variation over the time exhibits a naturally harmonic manner which is in compliance with the temperature gradient as seen in Figure 4.10.

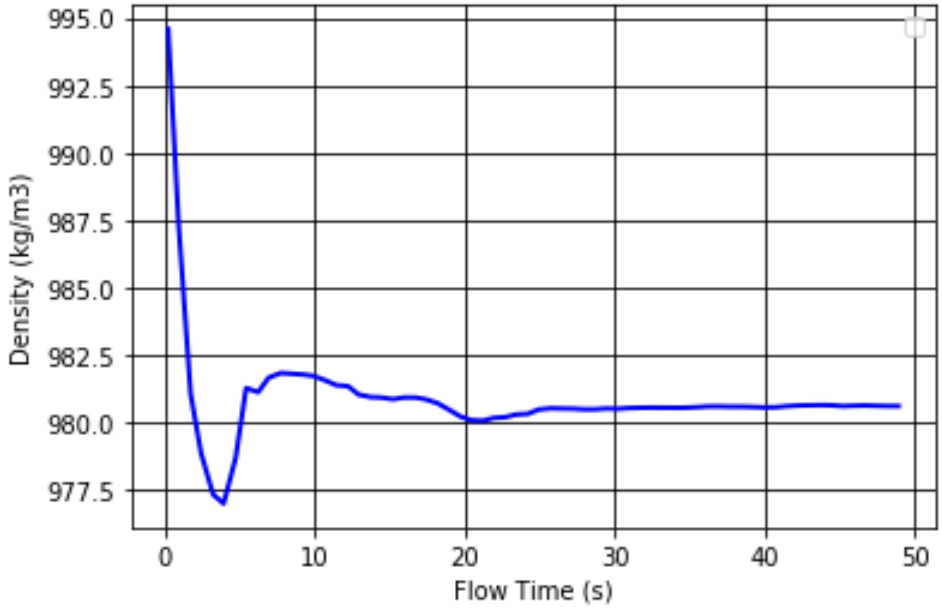

Figure 4.10 : The time dependence of density at the referenced location between B1 and C1 fuel elements.

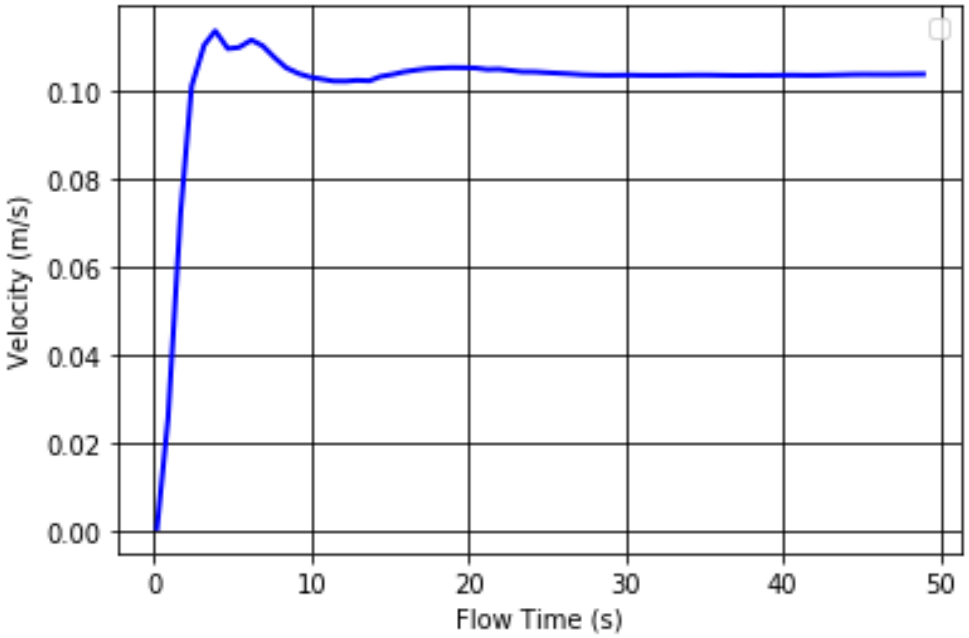

Figure 4.11 : Velocity-time dependence at the referenced location

Furthermore, Figure 4.11 shows that the fluid motion is accelerated by the acting gravitational force on less dense water molecules that is consistent with the physical concept of natural convection phenomena.

Although the simulation reaches a stable state, it is necessary to validate the results to make sure that all the modeling choices are appropriate. In order to validate the pool model, the comparison was performed with the experimental study described in [12]. The experimental study performed to measure coolant temperature distribution in the core at different locations for different reactor power levels. The measurements were carried out by inserting a portable thermocouple into foil insertion holes 2 and 3 shown in Figure 4.12.

The benchmarking was performed by extracting axial coolant temperature values form the CFD simulations for Hole 2 and 3 in Figure 4.12. The resulting graphs are displayed in Figure 4.13 and Figure 4.14 together with temperature measurement error of ±2 °C as reported in experimental study. The calculated temperature data is in good agreement with the experimental data at Hole 2 and Hole 3.

It should be noted here that in the pool model, the active fuel region of the fuel element lays between 0.78 and 1.16 m. Therefore, the rate of temperature increase in the coolant is high till 1.16 m in these figures. After this region comes the upper graphite plug in which heat generation is negligible as a result coolant temperature increase is extremely small if does not exist.

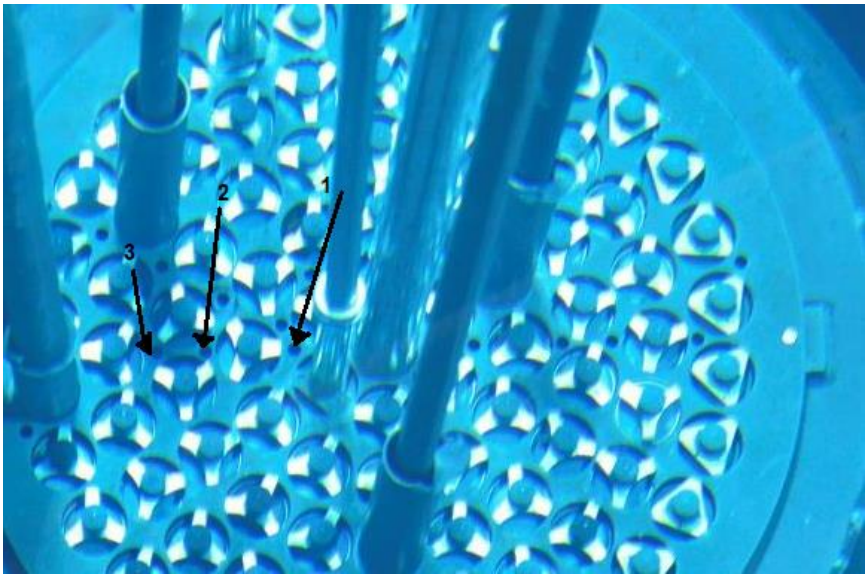

Figure 4.12 : The measurement locations of coolant temperature in the core at reference study [12].

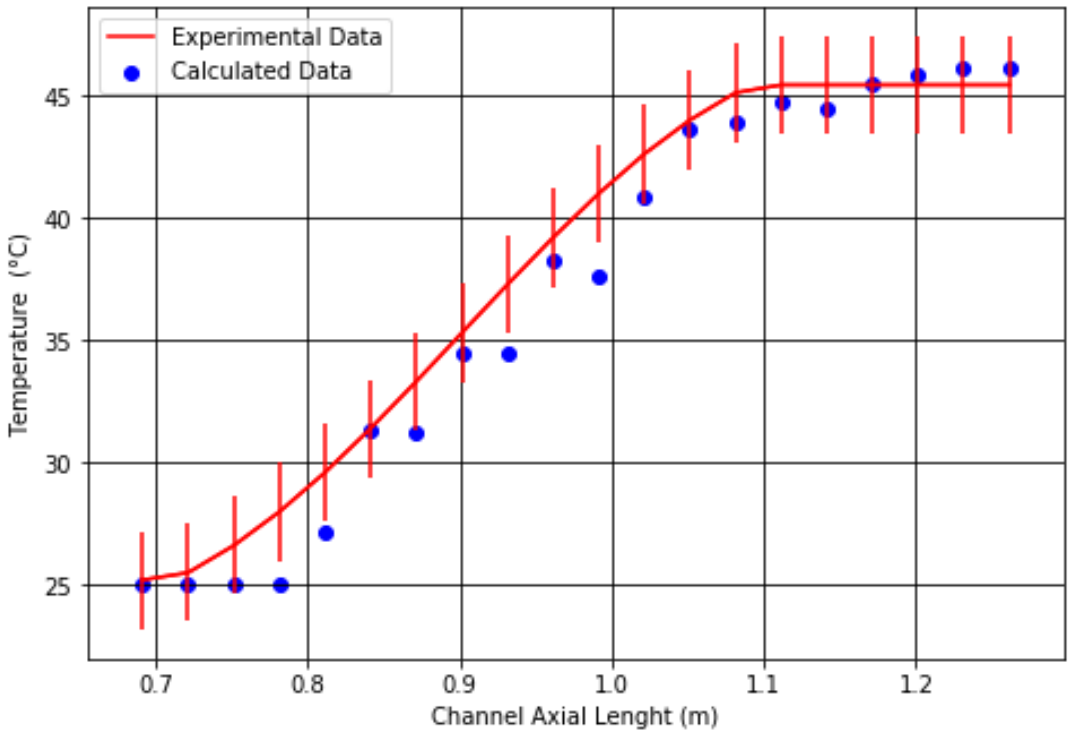

Figure 4.13 : Benchmarking of simulation result of axial coolant temperature profile at Hole 2.

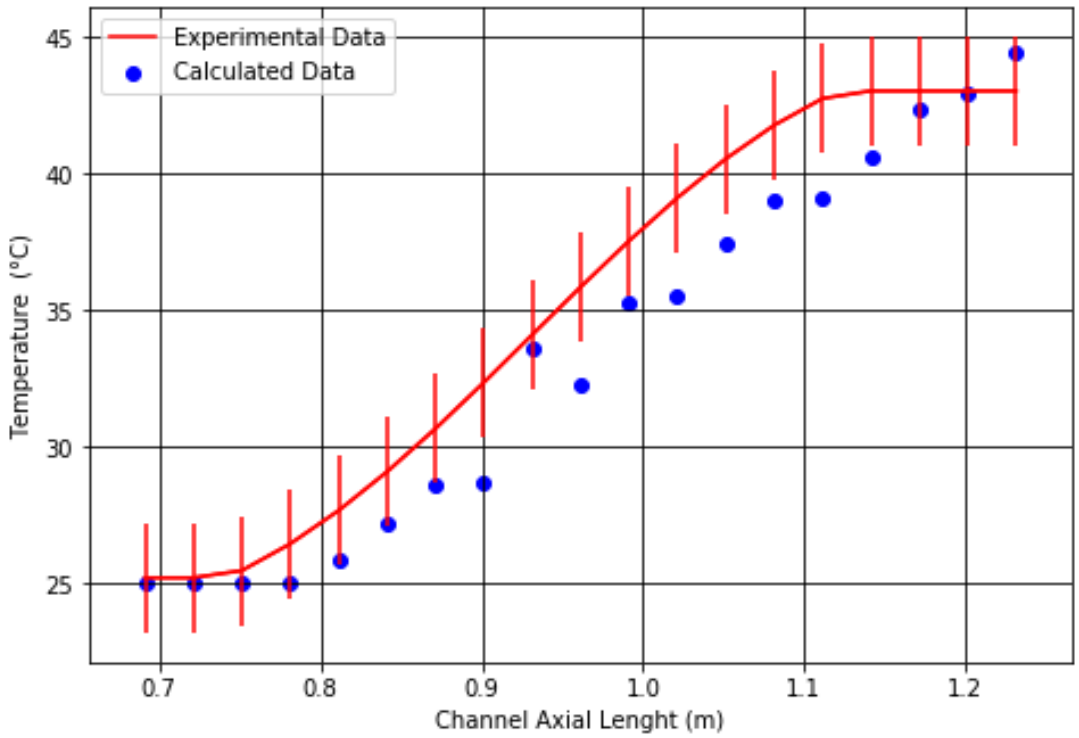

Figure 4.14 : Benchmarking of simulation results of coolant axial temperature profile at Hole 3.

In Figure 4.15 and Figure 4.16, the x and y direction velocity vectors in the cross sectional area at core axial center which corresponds to level at z=0.98 m from the active fuel region and corresponding coolant temperature profile are presented, respectively.

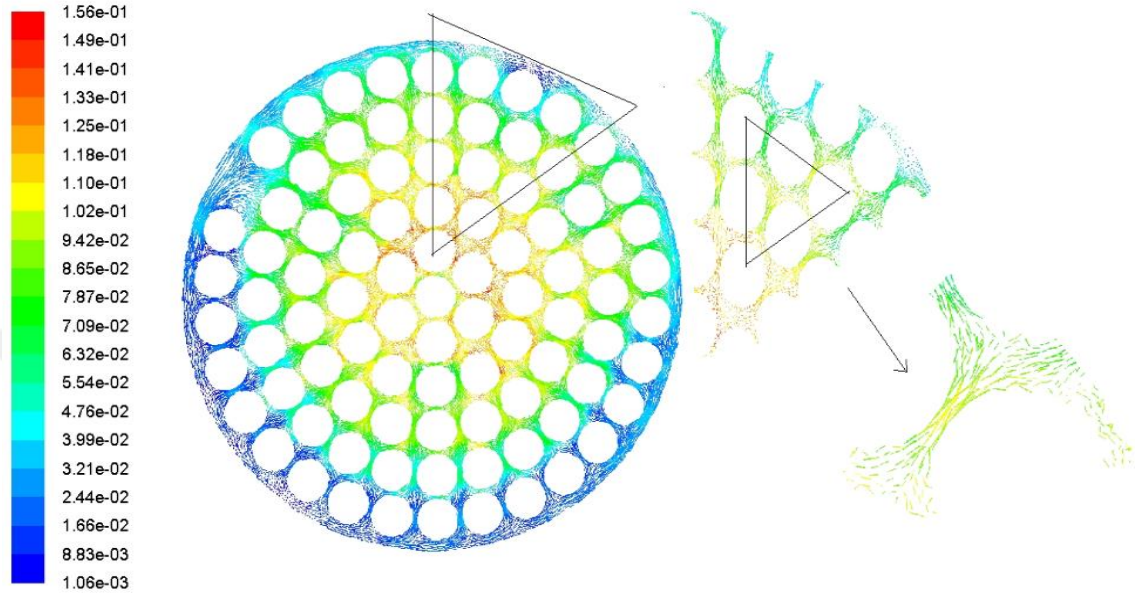

Figure 4.15 : x and y velocity (ms^{-1}) vectors in the cross sectional area at core axial center.

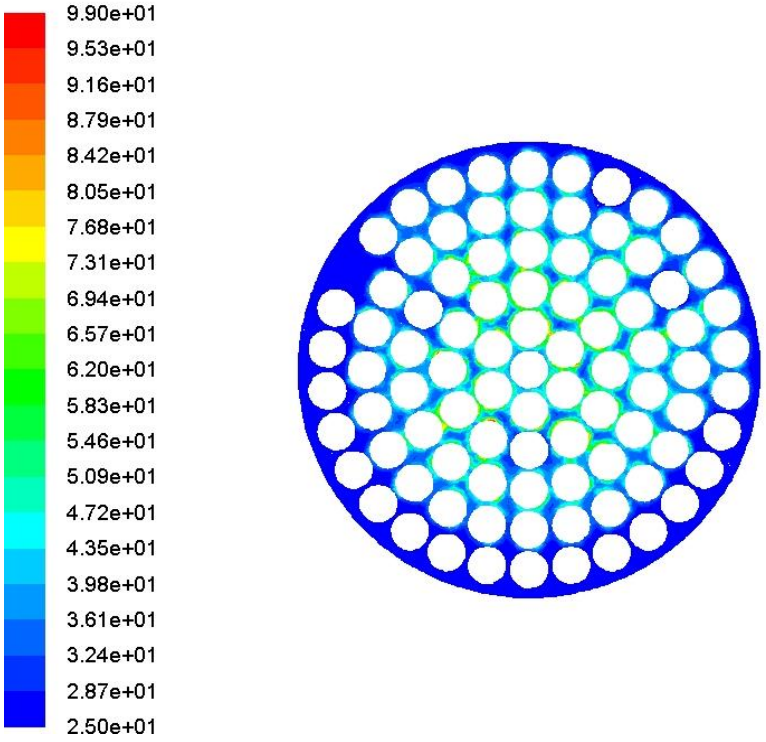

Figure 4.16 : Temperature distribution in the cross sectional area at core axial center.

It is seen clearly from Figure 4.16 that the temperature variation in the vicinity of the core radial center shows more diversity than other points in the core. Such variations cause the mixing flow and more turbulent dissipation at these locations since the lateral flows that come from the peripheral channels due to radial temperature gradient.

4.3.1.1 The effect of grid plates on thermal hydraulic parameters

The effect of grid plates on velocity field and temperature distribution had been investigated within the scope of this thesis. Because of that, another pool model was created without grid plates as well.

Figure 4.17 shows the pool and core velocity stream profiles when grid plates are included in the CFD model whereas Figure 4.18 shows the same profile without grid plates.

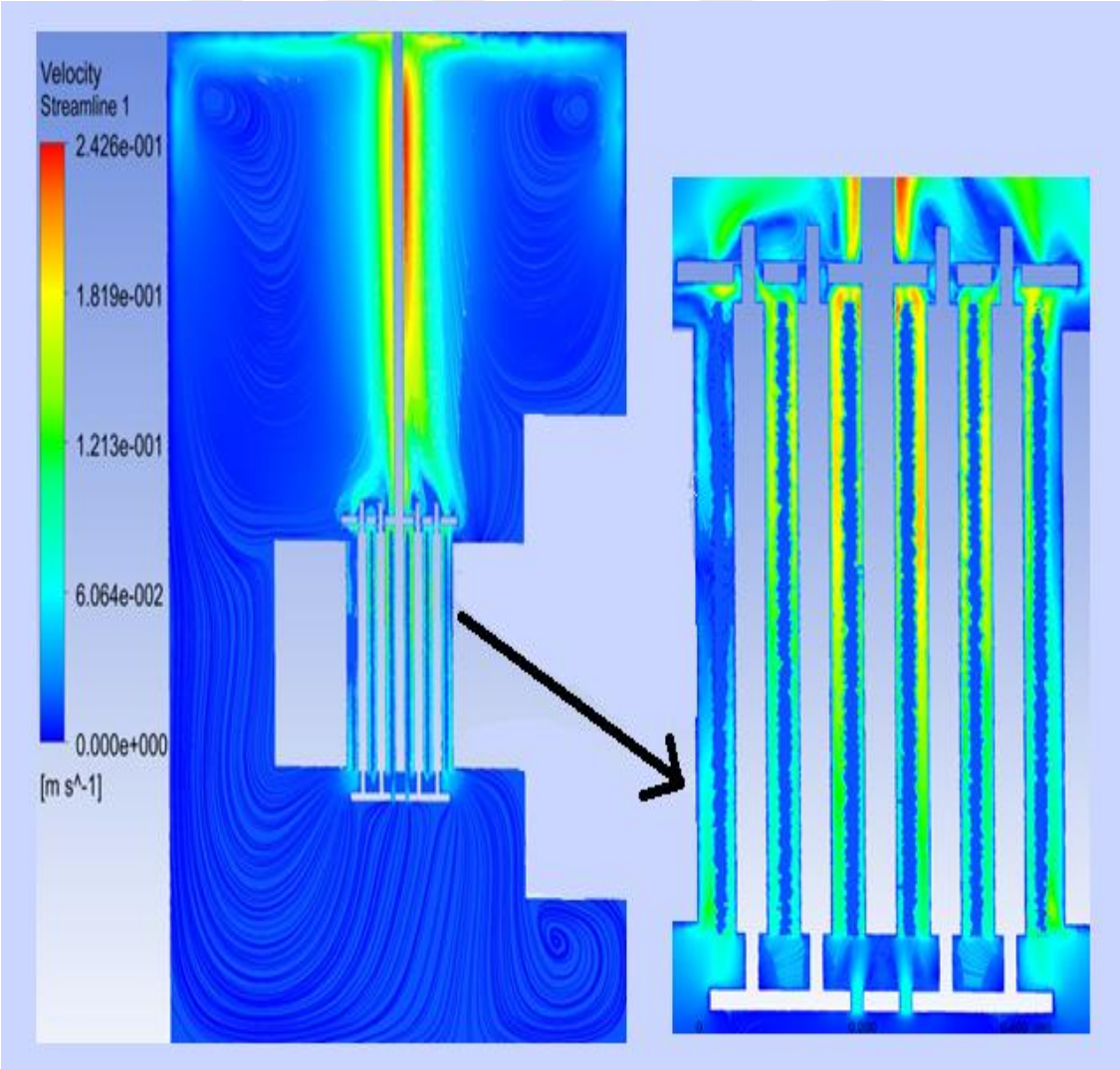

Figure 4.17 : Velocity stream profiles of coolant from pool model with grid plates.

The velocity streams exhibit similarly smooth behavior throughout the pool for both cases, but the velocity streams are more complex in core because of turbulence mixing due to grid plates. The grid plate sensitivity analysis shows that the flow is significantly suppressed by the grid plates. However, cooling performance in core is slightly affected from the grid plates in contrast to velocity magnitude which shows a substantial amount of drop if grid plates are present.

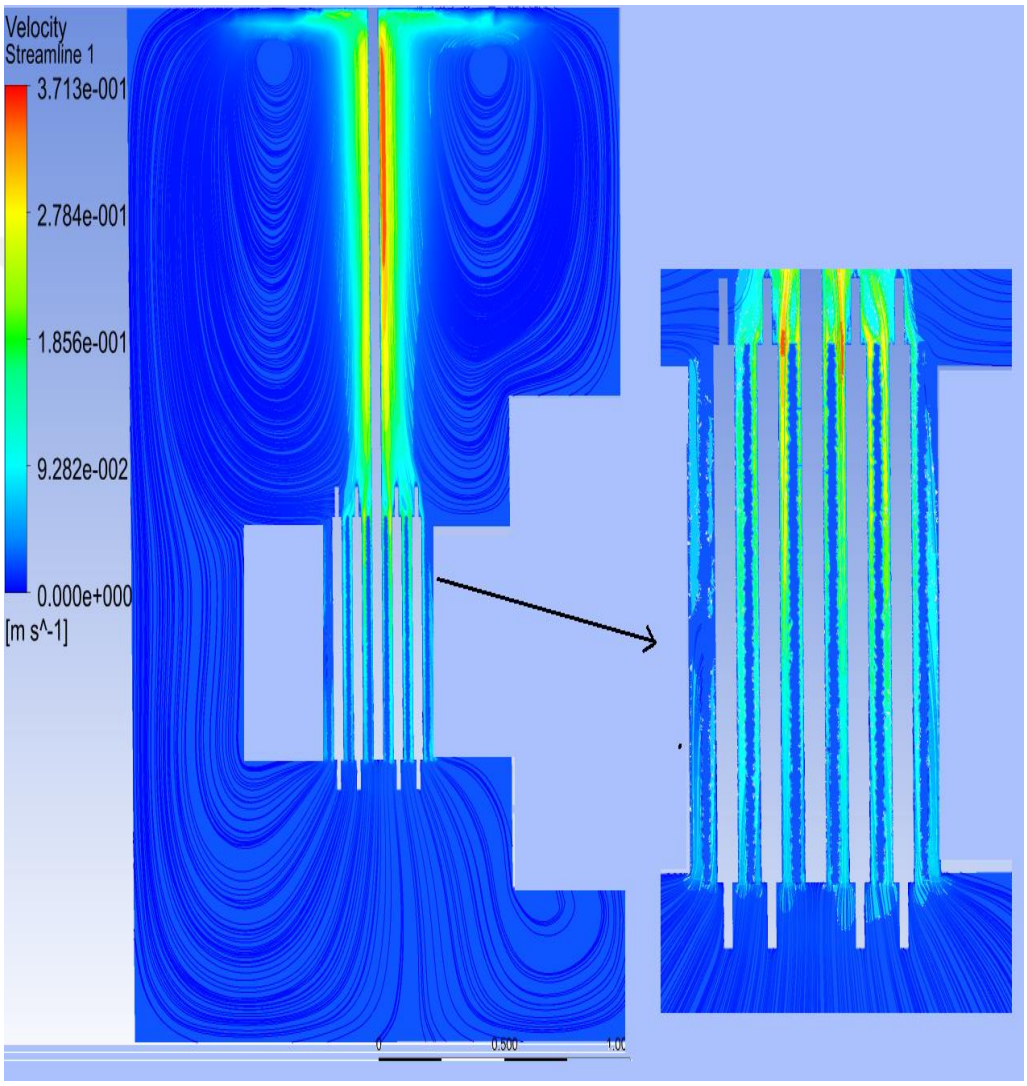

Figure 4.18 : Velocity stream profiles of coolant from pool model without grid plates.

In Table 4.5, the effect of grid plates on wall temperature is given by average coolant temperature in B ring. In this regard, the results show nearly 2 °C difference in comparison without grid plates. Consequently, the grid plates have not significant influence on temperature distribution, whereas velocity field of pool is reasonably affected from top grid plate.

Table 4.5 : The effect of grid plates on average wall temperature of different fuel rods.

Fuel rod	Temperature with grid plates (°C)	Temperature without grid plates (°C)
B1	54.635	52.998
B2	54.127	51.778
B3	52.252	51.529
B4	52.462	49.781
B5	50.526	48. 483
B6	52.516	50.055

Figure 4.19 indicates that the velocity magnitude is very low at a position right above the top grid plate compared to the same point in the core without grid plate. This drastic change of velocity out of the core is important for the rise time of activation product Nitrogen-16 (^{16}N) which has 7.4 s half life. Because the presence of grid plate actually increases the rise time therefore reduces the dose at the pool surface.

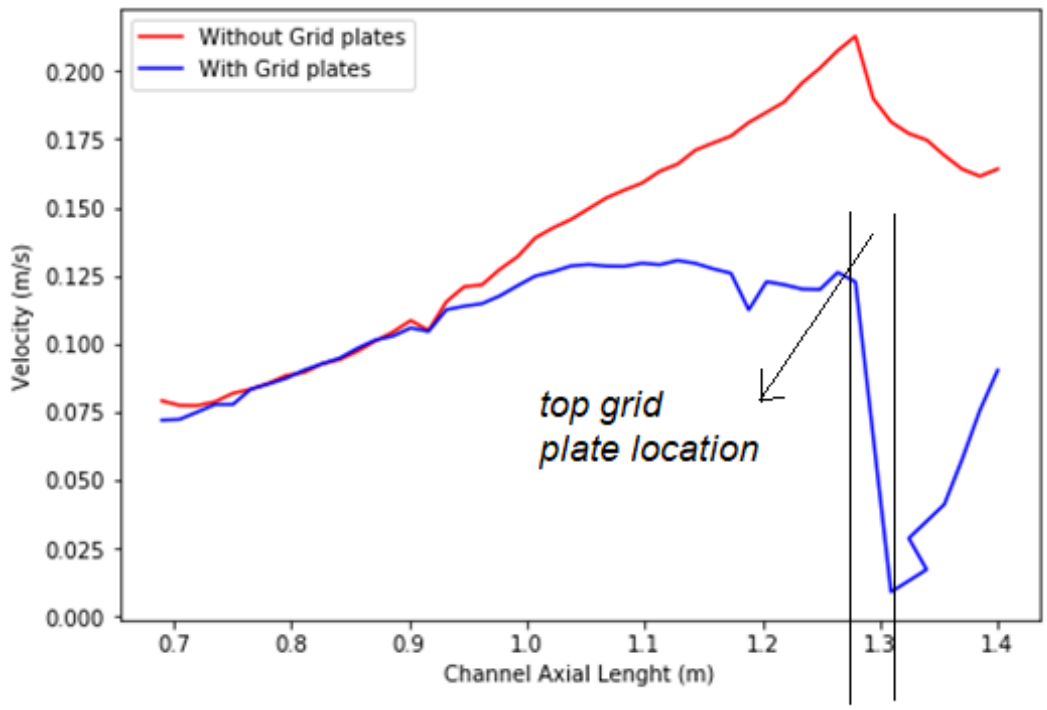

Figure 4.19 : The effect of grid plate on axial velocity in hole 1.

One of the objectives of CFD pool modelling is the estimation of core inlet velocity profile and core outlet pressure distributions to use core modelling simulation coming afterwards.

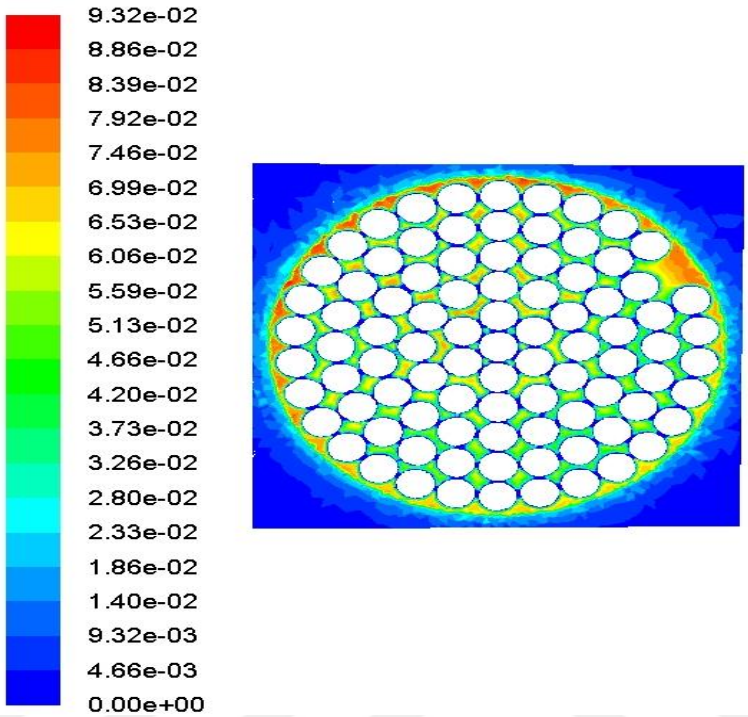

Figure 4.20 : The core inlet velocity (ms^{-1}) profile from pool model.

Nearly stable URANS velocity profile prediction in Figure 4.20 is used as velocity inlet boundary conditions at core inlet at the second stage calculations. The corresponding static pressure distribution on core outlet is shown by Figure 4.21.

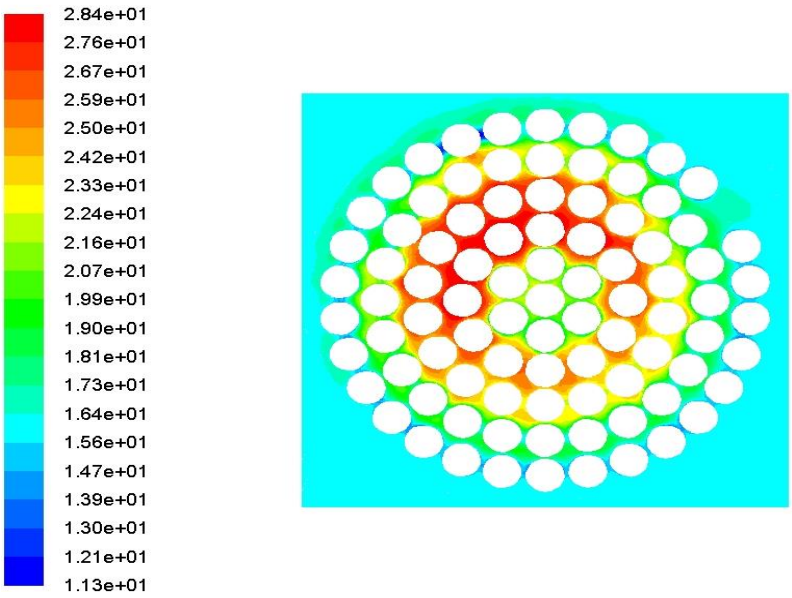

Figure 4.21 : Core out pressure (Pa) distribution from pool model.

4.3.2 TRIGA core model

In this section, the conjugate heat transfer modelling is employed to simulate multilayer heat conduction transfer within the fuel element as well as heat transfer to coolant.

The computation domain was considered as containing only inside of the graphite reflector. In this regard, the fluid domain was modelled by cutting all the core structure in the pool model, but keeping fuel elements as solid domain. To provide comprehensive thermal analysis for fuel elements, all the components of the fuel element (top and bottom graphite plugs, stainless steel clad, zircon central rod, and fuel meat) was modeled as in Figure 4.22. Furthermore, solid to solid interfaces were created to provide heat flow between two adjacent solid domains.

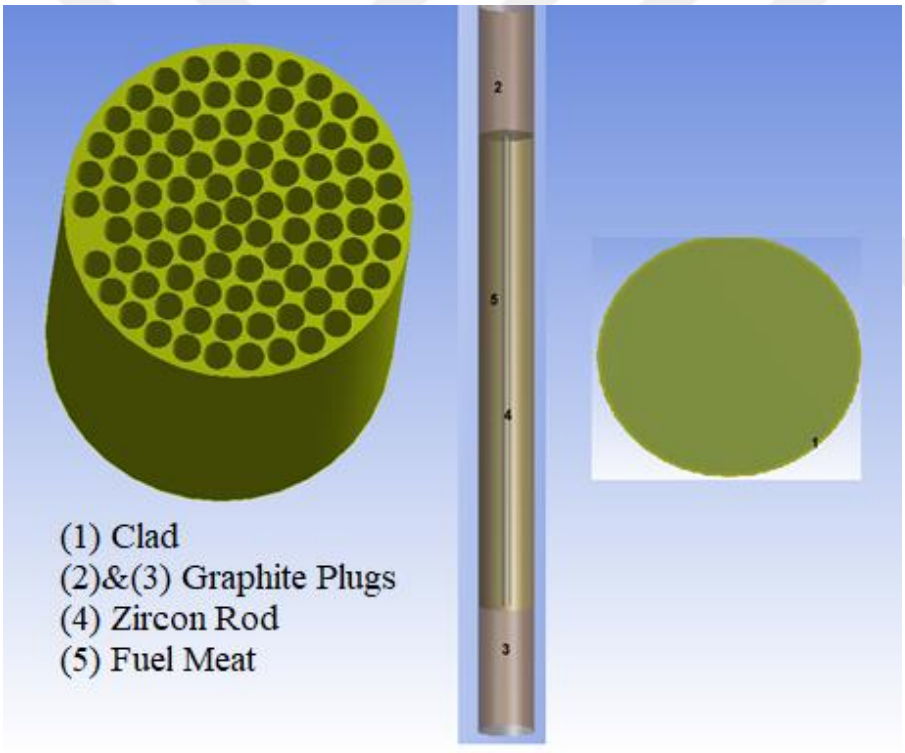

Figure 4.22 : Schematic view of core model; fluid domain (left), front view of a fuel element (right).

In the conjugate heat transfer analysis, the heat transfer across clad to coolant was performed using natural convection physical model. In this respect, the same numerical set up procedure in the previous section was established as given in Table 4.4. As mentioned before, the velocity profile from the pool model (Figure 4.20) was

assigned as a velocity inlet boundary condition. Furthermore, inlet coolant temperature was considered as 25 °C since the temperature through the core inlet is almost constant.

Another important aspect in core modelling is the contribution of grid plates on the flow cooling rate as discussed in Section 4.3.1.1. Therefore, the static pressure profile of the section under the top grid plate (Figure 4.22) was used as pressure outlet boundary condition.

Regarding thermal boundary conditions, energy source was given by the volumetric heat source defined in fuel meat cell zones (Figure 4.22 (5)) instead of heat flux boundary condition. In addition, the volumetric axial power distribution in all 69 fuel elements was specified by using user defined functions. Sample UDF is provided in Figure A.2 in Appendix A.

To ensure heat flow through the various fuel parts, thermo-physical properties such as thermal conductivity, specific heat capacity, and density of all material should be defined. In order to tackle this issue, temperature-varying thermal conductivity was specified by using user defined function for all fuel materials to demonstrate thermo-physical behaviors of TRIGA fuel against the temperature change (Figure A.3 in Appendix A). However, the other thermal properties of fuel element parts were taken as constant shown in Table 4.6 [54], [55].

Table 4.6 : Thermo-physical properties of parts of fuel elements.

Material	Thermal Conductivity (W/m K)	Density (kg/cm^3)	Heat Capacity (J/kg K)
Fuel (UZrH)	$k(T)=\left[12.5-2.4\left(1-\frac{T}{1000}\right)+1.5\right]\times 1.730735$	6040	340
Clad (SS)	17	7890	500
Central Rod (Zr)	23	6490	281
Graphite Reflector (C)	80	1600	710

Time dependent URANS solution was performed until the flow became steady. The result of conjugate heat transfer modelling was validated with measured fuel centerline

temperature from instrumented fuels at B1 and F9 positions seen in Figure 4.2 at 250 kW full power operation. The result of benchmarking showed that the computed centerline temperature data of instrumented fuel elements matched very well with the measured data (Table 4.7).

Table 4.7 : Benchmarking of fuel temperature for instrumented fuel elements.

Fuel Rod	CFD Simulation (°C)	Experimental Result (°C)	% Error
B1	238.13	240	0.77
F9	140.86	140	0.61

This analysis gave opportunity to calculate fuel temperatures in all 69 fuel elements accurately which has not been achieved before. The temperature distribution throughout the core axial center is illustrated in Figure 4.23.

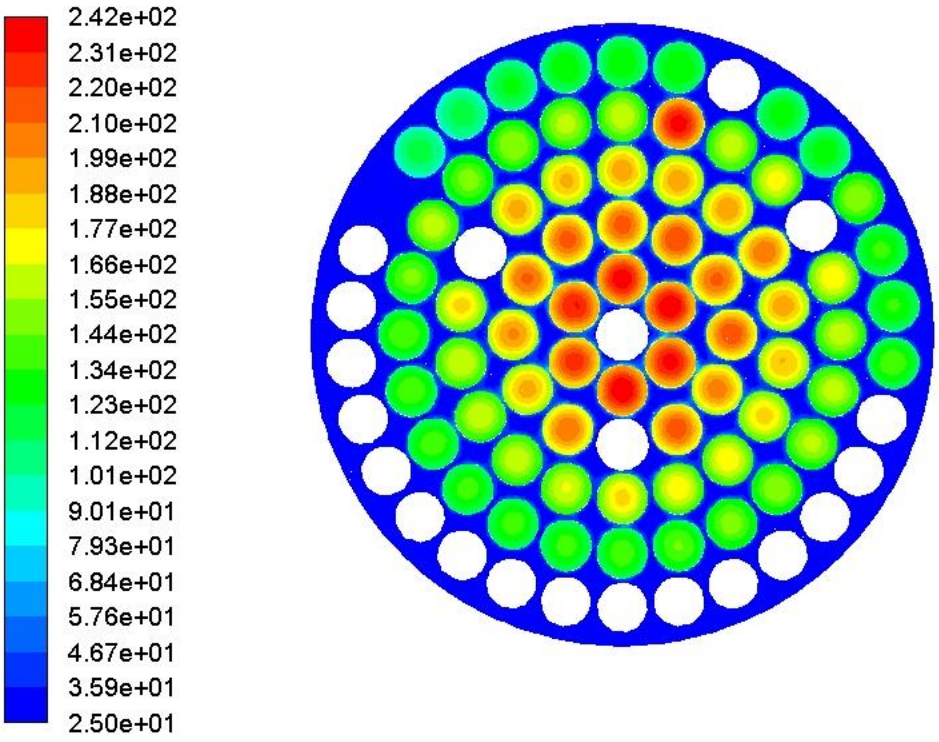

Figure 4.23 : Fuel element temperature (°C) distribution of ITU TRIGA Mark II reactor core at axial center plane.

Figure 4.23 shows that the highest fuel temperature in the core is around B ring since the fuel elements in this ring have the highest enrichment in the core. It was already shown in Section 4.2 that power profile is higher at the core radial center due to enrichment of fuel elements. Validated CFD core model results demonstrated that the

fuel centerline and clad temperatures are in acceptable margin[2] under normal operating conditions. The radial maximum individual temperature of the hottest fuel elements can be seen in Table 4.8.

Table 4.8 : Fuel radial direction maximum temperature values.

Fuel Rod	Fuel Centerline Temperature (°C)	Fuel Surface Temperature (°C)	Clad Outer Temperature (°C)
B1	238.13	194.05	180.91
B2	241.42	195.32	181.57
B3	235.18	191.74	178.32
B4	243.28	197.44	184.23
B5	227.25	184.71	172.61
B6	232.65	189.11	176.71

The maximum temperatures of all fuel elements and average fuel meat temperatures are given in Table B.1 in Appendix B.

The radial temperature distribution at the axial centerline at z=0.98 m of the hottest fuel element which is at B4 position is illustrated in Figure 4.24.

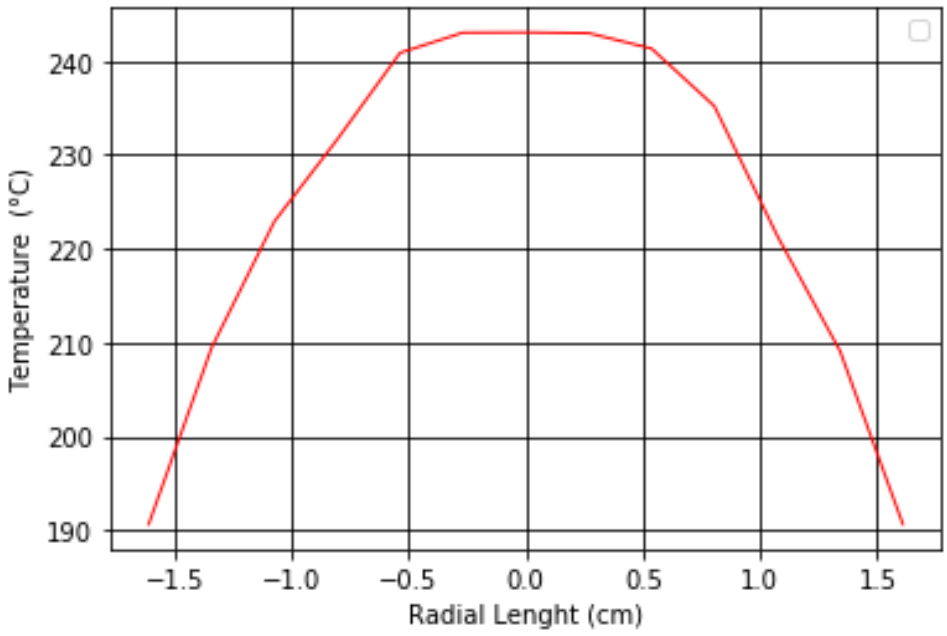

Figure 4.24 : The radial temperature profile of hottest fuel element at axial centerline.

[2]"Operational safety criteria – Criteria specific to the fuel design and provided by the fuel vendor as part of the licensing basis. Operational criteria ensure that safety criteria are not violated." [59]

As can be seen in this figure, the temperature does not change along the zirconium rod. In addition, since the thermal conditions are symmetric along the zirconium rod, the temperature decreases radially outward in parabolic trend.

Figure 4.25 presents the axial temperature distribution of the hottest channel (B-ring) fuel elements. The figure confirms the cosine shape power density which is the ideal design for neutronic-thermal-hydraulic interactions for a fuel element.

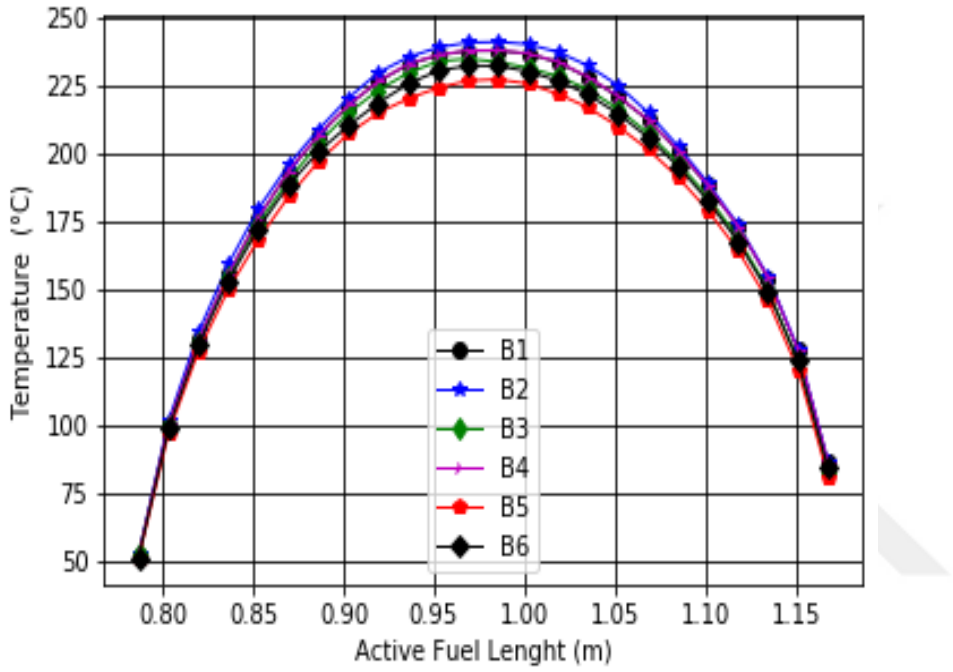

Figure 4.25 : The axial temperature profile of hottest channel (B-ring) fuel elements.

4.3.2.1 Pool boiling phenomenon in reactor pool

The pool boiling phenomenon in the core was numerically investigated, too. According to Nukiyama pool boiling curve in the Figure 4.26, the excess temperature known as the difference between wall temperature $T_{wall,}$ and the saturation temperature of water T_{sat} is below 5 °C at the natural convection boiling stage [56].

The fuel wall temperature results of CFD simulations were extracted to analyze pool boiling in reactor core (Figure 4.27). Since the saturation temperature of coolant $T_{sat,}$ is equal to 99.97 °C at a pressure of 1 atm [58], Figure 4.27 indicates that the pool boiling regime in ITU TRIGA core is at single phase regime or convective stage since the ΔT_{sat} is generally below 5 °C. However, the wall temperature with a value of 105 °C somewhere on the wall of the central fuel elements exceeds the transition point A in Figure 4.26. This point is called as Onset of Nucleate Boiling (ONB) in literature.

On the other hand, the subcooled boiling flow regime arises on ITU TRIGA core when the bubble formation occurs locally at these points, while the bulk temperature remains below saturation temperature.

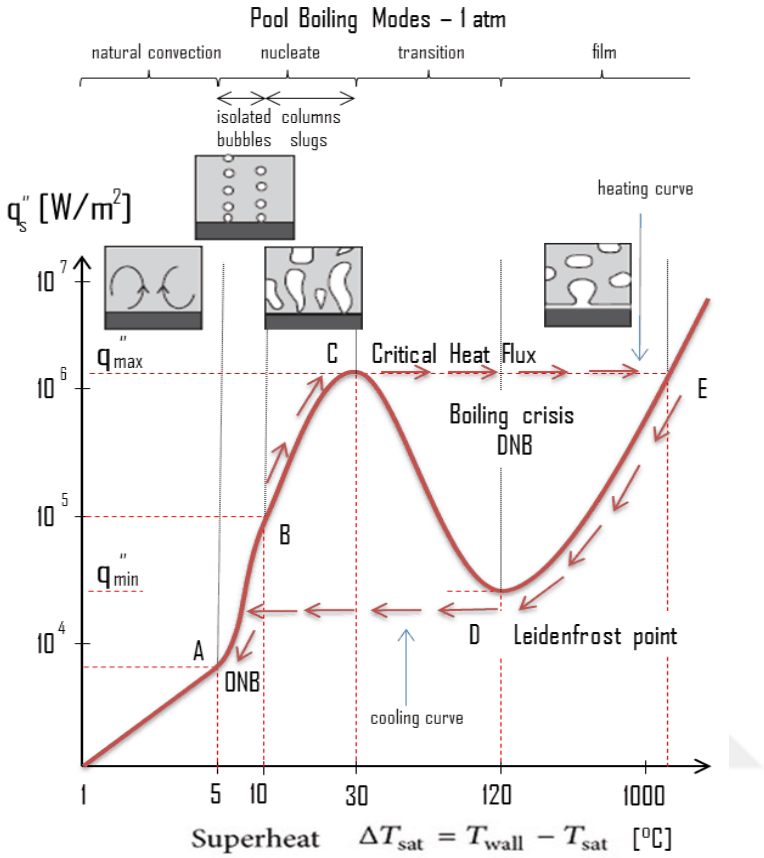

Figure 4.26 : Pool boiling curve [57].

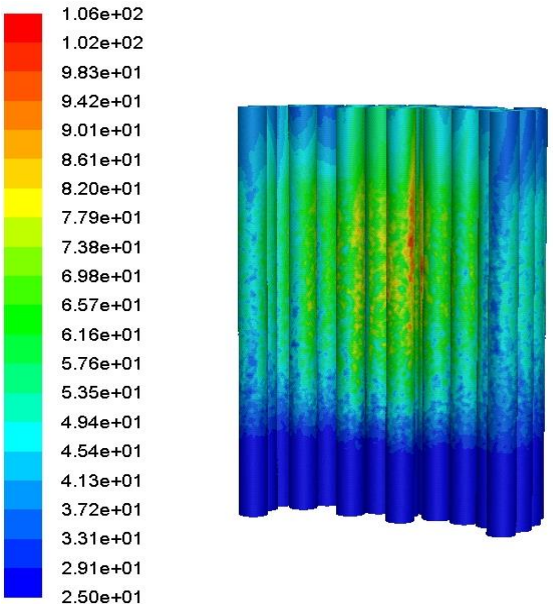

Figure 4.27 : Wall temperature (°C) distribution of fuel elements.

4.3.2.2 The effects of thermal hydraulic parameters on neutronic behavior

It is a known fact that thermal hydraulic parameters affect the neutronic behavior of a reactor. The neutronic model used in Section 4.2 was generated by using average temperatures for fuel elements and coolant. Thermal hydraulic analysis provided valuable information about the coolant and fuel element temperature distributions in the core. In MCNP model, it is possible to use different temperatures for all components in the core. In last section of the thesis, thermal hydraulic analysis results were used not only to investigate the effect of abovementioned distributions but also to improve neutronic model of ITU TRIGA Mark II research reactor.

Four cases described below were considered for the investigation at 250 kW full power. The base case (Case 0) having average temperature for all fuel elements and uniform coolant temperature and density in the pool has excess reactivity of 1.609 $.

Case 1: The effect of fuel temperature

The average temperature for each individual fuel element given in Table B.1 in Appendix B were inserted in MCNP model by using TMP card. The cross-section temperatures that were taken from ENDF-B/7 data library was selected as close as possible to TMP card values.

Case 2: The effects of both the coolant density and fuel temperature

On top of Case 1, coolant density in the core was modified while keeping the coolant temperature same as in the base case. Five subchannels were designed by taking into account the radial position of the fuel elements and geometry modeling used in MCNP input (Figure 4.28) As a result, the average coolant temperatures in each subchannel were calculated and corresponding water densities were found from literature. The density values used for Case 2 MCNP input are displayed in Table 4.9.

Table 4.9 : Thermal properties of coolant of subchannels.

Subchannel	Average Temperature (°C)	Average Density (kg/m^3)
A-B	40.307	989.302
B-C	37.464	995.606
C-D	36.274	991.185
D-E	34.748	991.926
E-F	31.592	993.226

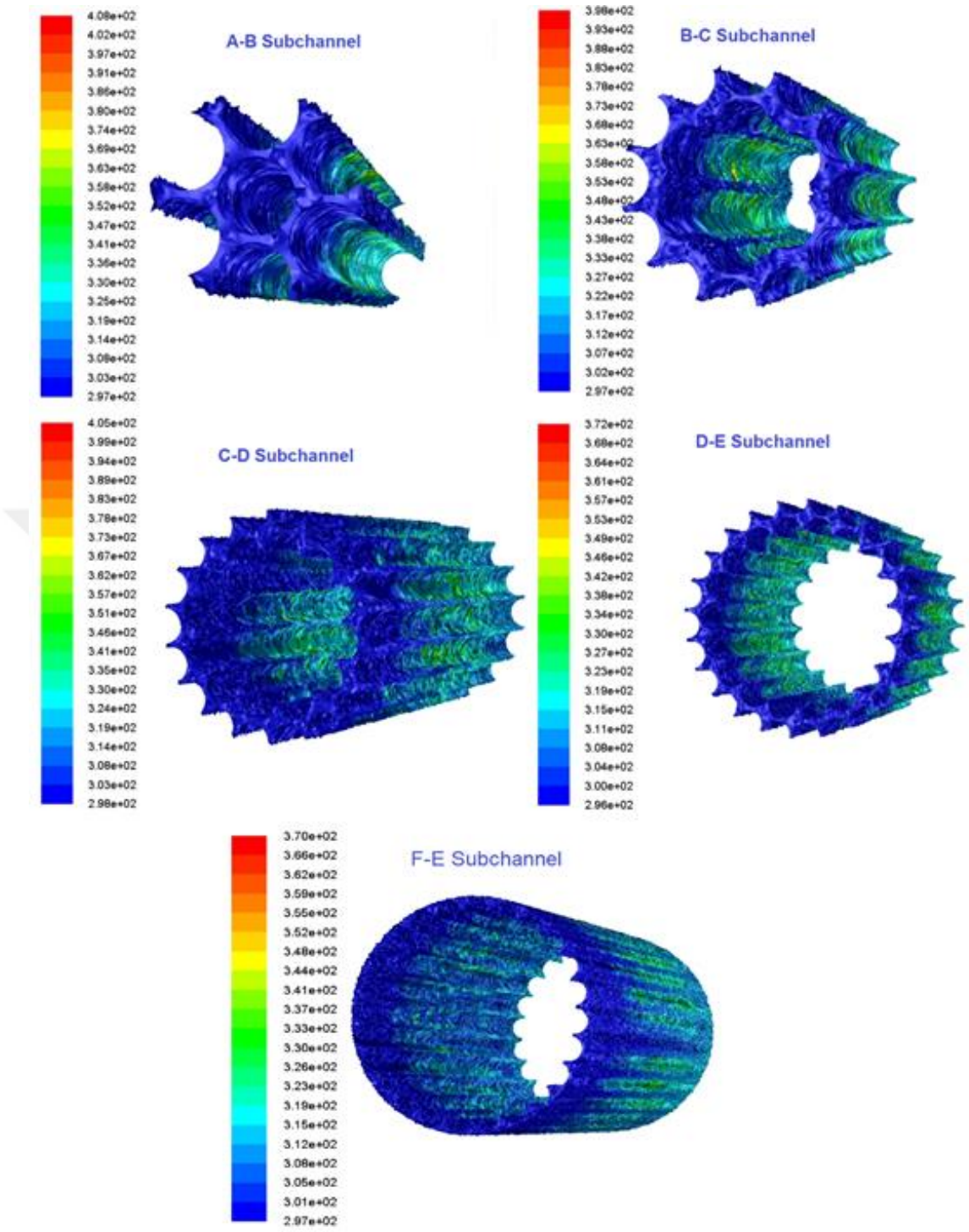

Figure 4.28 : Coolant temperature (°C) distribution in subchannels.

Case 3: The effects of average coolant density, fuel temperature, and coolant temperature

On top of Case 2, temperature of coolant in subchannels were also updated according Table 4.9.

All the cases are summarized in Table 4.10.

Table 4.10 : Cases for investigation of thermal hydraulic parameters on neutronic behavior.

Cases	T_{fuel} value in core	ρ_{colant} value in core	$T_{coolant}$ value in core
Case 0	Core average	Core average	Core average
Case 1	Individual for all fuel elements	Core average	Core average
Case 2	Individual for all fuel elements	Individual for all subchannels	Core average
Case 3	Individual for all fuel elements	Individual for all subchannels	Individual for all subchannels

The core excess reactivity results for all cases were compared in order to clarify the effect of fuel temperature, coolant temperature, and coolant density. Table 4.11 indicates that from the base case (Case 0) to Case 1 where only fuel temperatures were modified, reactivity drops from 1.609 $ to 1.594 $. This occurs due to of the Doppler Broadening effect that arises from dependence of neutron cross-sections on temperature variation in the fuel.

Table 4.11 : The effects of thermal hydraulic parameters on neutronic behavior.

Cases	Reactivity ($)
Case 0	1.609
Case 1	1.594
Case 2	1.557
Case 3	1.563

The effects of density and temperature change in coolant could be discussed with comparing Case 1 with Case 2 and Case 2 with Case 3. As seen in Table 4.11, the density refining of coolant has given negative reactivity response. On the contrary, coolant temperature refining resulted in positive reactivity response. As stated before, UZrH TRIGA fuel has self-moderating characteristics therefore self-thermalization because of the Hydrogen in fuel material. Moreover; molecular bonding of Hydrogen in ZrH differs from Hydrogen bound in water molecules and it causes different neutron thermalization characteristics in Hydride, Uranium, and water [19]. At the beginning of operation, an over-moderation occurs in core as the water density is high. However, water density decreases over time due to heating, the moderating capability decreases which will insert negative reactivity. The coolant density has more profound effect than coolant temperature on reactivity.

5. CONCLUSIONS AND RECOMMENDATIONS

In this thesis, the multi-physical approach was used to model ITU TRIGA Mark II research reactor to provide comprehensive 3D neutronic and thermal hydraulic analysis.

In order to perform thermal hydraulic analysis of the research reactor, it is necessary to know heat generation in each individual fuel element. This part of the research can be done by using neutronic modeling. In this respect, 3D Monte Carlo neutronic model previously generated at Energy Institute by Asst. Prof. Dr. Senem Şentürk Lüle with MCNP 6.2 code was modified. F4 tally ad FM multiplier options were used. The main issue in nuclear fuel is that the heat generation in the element has axial distribution. Therefore, another manipulation was performed to divide each fuel elements into 19 axial segments with FMESH tally option of the code. According to power generation results, the average power generation per element is equal to 3.67 kW/element whereas the maximum and minimum power generation per element are equal to 5.64 and 2.08 kW, respectively. The heat flux and the volumetric heat generation was calculated for each fuel element to provide thermal boundary conditions for the CFD modelling. Since axial heat generation option is not included in FLUENT code by default, user defined function feature of the code was used. The volumetric heat generation and heat flux data were converted into axially varying second order polynomials with cure fitting. This procedure was applied for all 69 individual fuel elements.

The thermal hydraulic analysis was performed by using FLUENT code. In this regard, natural convection flow and conjugate heat transfer analysis were performed. Because of the size of the reactor tank (pool), the number of mesh required for the simulation of natural cooling in the pool and for the simulation of detailed conjugate heat transfer were extremely high. As a result, in order to manage the simulations in a reasonable time thermal hydraulic analysis was divided into two stages.

Firstly, The TRIGA pool was modelled without any major assumptions as accurately as possible. Thus, the effects of major flow restrictions stem from the grid plates and

other core components had been taken into account. As part of numerical model set up, the temperature dependent density was used for natural convection as well as the appropriate solver settings. URANS simulation was performed till all parameters reach steady state. In this regard, the CFD pool model was benchmarked against experimental data. The results of simulation showed good agreement with measurement coolant temperature values. According to CFD pool model, water enters the core at 25 °C and leaves nearly at 48 °C at the hottest channel. In addition, fuel element at B4 position has the maximum wall temperature 109 °C since it has maximum heat generation by fission which is due to its enrichment level.

Furthermore, the effect of grid plates, which are responsible for holding fuel elements in place, on cooling performance and velocity streamlines in the pool tank was investigated by creating another pool model without grid plates. The results showed that the grid plates mostly affect the velocity distribution and magnitude. The velocity magnitude drops at the core outlet because of grid plates. This decrease in velocity increases the rise time of the activation product Nitrogen-16 and reduces the dose at the top of the reactor tank.

At the second stage, the conjugate heat transfer method was used to provide coupled solution for conduction heat transfer in fuel elements and natural convection heat transfer in fluid. In this regard, in general, grid plates are not included and only the fuel elements in the reflector structure are modeled. However, as discussed above, grid plates have important effect on velocity distribution and pressure drop in the core. The approach we used in this thesis is different and unique. The velocity field profile at core inlet where bottom grid plate positioned and the pressure distribution profile at core outlet where top grid plate positioned were extracted from the pool model simulations performed at the first stage and implemented in the core model as boundary conditions. As a result, model was completed without any sacrifice of physical representation of flow characteristics. By this way, the thermal hydraulic parameters of core had been obtained numerically in detail.

The core model was validated and verified with fuel temperature results of instrumented fuel elements at 250 kW power recorded in logbook of ITU TRIGA Mark II research reactor. The benchmarking showed that, the percent error between simulation and experimental results below 1 % indicating excellent agreement.

The results showed that the maximum fuel temperature in the core is 243 °C in the fuel element at B4 position that has the highest heat generation. The maximum clad outer temperature of B4 fuel element is 184 °C. Consequently, it can be said that operational safety limits are not exceeded at full power operation.

In addition, the pool boiling phenomenon had been numerically investigated at the ITU TRIGA core. According to pool boiling curve and simulation results, single phase regime or natural convective stage exits in the core since the difference between the clad outer temperature and saturation temperature is generally below 5 °C. Nevertheless, the clad outer temperature reaches maximum 109 °C at some points that requires exceeding the transition point. Therefore, the subcooled boiling flow regime arises on ITU TRIGA core when the bubble formation occurs locally at these points, while the bulk temperature remains below saturation temperature.

Finally, the effect of thermal hydraulic parameters on neutronic behavior had been investigated by using these parameter values from the CFD simulations in MCNP neutronic model. In this regard, it can be said that increase in fuel temperature and the decrease in density of coolant insert negative reactivity in the core because of Doppler Broadening and decrease in moderation capacity, respectively.

In conclusion, this thesis provides the temperature profile in all 69 fuel elements in the core and in coolant which are calculated accurately with verified and validated models. These neutronic and thermal hydraulic models can be used both steady state core parameter estimations and prediction of neutron spectra for in core experiments.

As a further study, continuous energy neutron cross section and kernel scattering thermal data at relevant temperatures can be achieved with appropriate software to make neutronic model more accurate. In addition, the temperature information of fuel elements can lead new studies related with fuel performance.

REFERENCES

[1] **Nuclear Energy Agency.** (2008). *System Code Models and Capabilities in Seminar on the transfer of competence, knowledge and experince gained through CSNI activites in the field of thermal hydraulics,* Pisa, Italy OECD

[2] **Nuclear Energy Agency.** (2007). *COTSON Installations, Best Practice Guidelines for the use of CFD in Nuclear Reactor Safety Applications,*OECD.

[3] **Nuclear Energy Agency**. (2015). *Assessment of CFD Codes for Nuclear Reactor Safety Problems*, OECD.

[4] **Korea Atomic Energy Research Institute.** (2005). *The Numerical Nuclear Reactor for High Fidelity Integrated Simulation of Neutronic,Thermal-Hydraulic, and Thermo-Mechanical Phenomena*, Daejeon

[5] **Weber, D. P., Sofu, T., Yang, W. S.** (2007). High-Fidelity Light Water Reactor Analysis with the Numerical Nuclear Reactor. *Nuclear Science and Engineering,* 155:3, 395-408, doi: 10.13182/NSE07-A2672

[6] **Sarikaya, B. & Tombakoglu, M.** (2000). Preleminary neutronic design of TRIGA MARK II reactor, *I. Eurasia conference on nuclear science and its application : presentations*, , Izmir, Turkey.

[7] **Turkmen, M. & Colak, U.** (2014). Analysis of ITU TRIGA Mark II Research Reactor using Monte Carlo method, *Progress in nuclear Energy,* 77, 152-159, doi:10.1016/j.pnucene.2014.06.015

[8] **Ozkul, E., H.** (2000). *Thermal-Hyrdrualic Analysis of ITU TRIGA- Mark -II Reactor*, (Master Thesis). Istanbul Technical University, Nuclear Energy Institute Istanbul.

[9] **Ozkul, E., H. & Durmayaz, A.** (2000). A parametric Thermal-Hydraulic analysis of I.T.U. TRIGA MARK-II reactor, *I.T.U. Institute for Nuclear Energy,* Istanbul Technical University.

[10] **Ozkan, I**. (1995). *ITU TRIGA Mark -II Reaktörünün iki Boyutlu Bilgisaya Simulasyonu,* (Master Thesis). Istanbul Technical University, Nuclear Energy Institut, Istanbul.

[11] **Url-1** <http://www.triga.itu.edu.tr> Date Retrieved: 10.06.2020

[12] **Buke,T. & Yavuz, H.** (2000). Thermal Hydraulic Analysis of the ITU TRIGA Mark-II Reactor, *I. Eurasia Conference on Nuclear Science and Its Application*, Izmir, Turkey

[13] **Babitz, P., Choe, D., Jevremovic,T.** (2013). Feasibility study of the University of Utah TRIGA reactor power upgrade Part II: Thermohydraulics and Heat Transfer Study in Respect to Cooling System Requirements and Design. *Nuclear Technology & Radiation Protection,* 28, 352-361, doi: 10.2298/NTRP1304352B

[14] **Babitz, P**. (2012). Thermal-Hydraulic analysis of the university of UTAH TRIGA reactor of higher power design, (Master Thesis), The University of UTAH, Nuclear Engineering.

[15] **Nazar, R. & KA, S.** (2018). The thermohydraulic analysis of the Bandung research reactor core with plate type fuel elements using the CFD code, *Jurnal Teknologi Reaktor Nuklir*, 20:3, 123-132, doi: 10.17146/tdm.2018.20.3.4626

[16] **Lianes, M. M., Miro, R., Reis,P.** (2011). Steady-State modeling of flow conditions of a TRIGA reactor using the CFD code ANSYS CFX, *International Nuclear Atlantic Conference* , Brazil.

[17] **Silva, V. V., Santos, A., Silva P. S.D, Pereira, C.** (2013). CFD simulation of IPR-R1 TRIGA subchannels fluid flow, *International Nuclear Atlantic Conference - INAC 2013*, Recife, PE, Brazil.

[18] **IAEA,** (2008). *Design of the Reactor Core for nuclear power plants -IAEA Safety Standards for protecting people and the environment*- Vienna

[19] **Boeck, H.** (2007) TRIGA Reactor Characteristics, *IAEA INIS, 39:10,* Austria

[20] **Seker, V., Thomas, J., W., Downar, T. J.** (2007) Reactor Physics simulations with coupled Monte-Carlo calculation and Computational Fluid Dynamics, *International Conference on Emerging Nuclear Energy Systems*, Istanbul, Turkey

[21] **Cordani, J.,N., & Uddin,R.** (2011). Nuclear Reactor Multi-Physics simulations with coupled MCNP5 and STAR-CCM+, *International Conference on Mathematics and Computational Methods Applied to Nuclear Science and Engineering*, Rio de Janeiro, RJ, Brazil.

[22] **Henry, R.** (2017). *Neutronic and Thermal Hydraulic coupling for simulations of the TRIGA Mark-II research reactor*, (Doctorate Thesis),University of LJUBLJANA, Faculty of mathematic and physics, Ljubljana,Slovenia.

[23] **Ganapol,B.D** (2008) Analytical Benchmarks for Nuclear Engineering Applications," Nuclear Energy Agency, (ISBN 978-92-64-99056-2)

[24] **Duderstadt, J. J., & William, M.R**. (1979). *Transport Theory*, New York: Wiley,.

[25] **Duderstadt, J. J., & Hamilton, L. L.** (1975). *Nuclear Reactor Analysis*, Michigan: Wiley

[26] **MCNP-TM–A General Monte Carlo N–Particle Transport Code**,(Version 6.2) [computer program], Los Alamos National Laboratory.

[27] **NJOY nuclear data processing system** (Version 12) [computer program], *Los Alamos National Laboratory*, Los Alamos National Laboratory.

[28] **Snoj,L. & Ravnik, M.** (2006) Calculation of Power Density with MCNP in TRIGA Reactor, *Nuclear Energy for New Europe*, Portorož,Slovenia

[29] **Zerovnik,G., Rodvratnik, M., Snoj, L**. (2014). On normalization of fluxes and reaction rates in MCNP criticality calculations, *Annals of Nuclear Energy*, 63, 126-128, doi: 10.1016/j.anucene.2013.07.045

[30] **Todreas, N., E., & Kazimi, M. S.** (2012) *Thermal-Hydraulics Fundamentals*, CRC Press: United States

[31] **Url-2** <https://www.afs.enea.it/project/neptunius/docs/fluent/html/th/node107.

html> Date Retrieved: 6.05.2020

[32] **Url-3** <https://en.wikipedia.org/wiki/Boussinesq_approximation_buoyancy> Date Retrieved: 11.03.2020

[33] **ANSYS, Inc**, (2009). Ansys Fluent User Guide.

[34] **Rodriguez, S.** (2019). *Applied Computational Fluid Dynamics and Turbulence Modeling, Practical Tools, Tips and Techniques*, Springer, 2019, pp. 121-191. Albuquerque, NM, USA

[35] **SODJA, J.** (2007). *Turbulence models in CFD,* (Master thesis) University of Ljubljana, Faculty for mathematics and physics, Ljubljana,Slovenia

[36] **Chance, C. M**. (2014) Partial Core Blockage simulation using COBRA-TF, (Master thesis) Texas A&M University,Nuclear Engineering,

[37] **Academic Research Fluent** (Release 18.2). [computer program],ANSYS inc.

[38] **ANSYS inc,** ANSYS Workbench Documentation, ANSYS Workbench Products Release Notes, U.S.A.

[39] **Url-4** <https://www.afs.enea.it/project/neptunius/docs/fluent/html/th/node373.htm.> Date Retrieved: 20. 03.2020

[40] **Url-5** <https://www.afs.enea.it/project/neptunius/docs/fluent/html/th/node361.htm.> Date Retrievied: 20. 03.2020

[41] **Fluent.Inc** (2003). *FLUENT 12:UDF Manual*, Centerra Resource Park

[42] **Fluent Inc,** *FLUENT 6.1: UDF Manuel,* Lebanon

[43] **SAR**, (n.d). Safety Analysis Report of ITU TRIGA MARK-II Research Reactor. *Institute of Nuclear Energy,* Istanbul Technical University

[44] **Buke,T & Yavuz H** (2000) Thermal-Hydrualic Analysis of the ITU TRIGA Mark-II, *I.T.U. Institute for Nuclear Energy,* Istanbul Technical University.

[45] **Stone, R. S., Sleeper, H. P., Ralp, H.** (2017) Transient Behavior of TRIGA, a Zirconium-Hydride,Water-Moderated Reactor, *Nuclear Science and Engineering,* 6:4 225-259, (1959-2017 repuplished)

[46] **IAEA** (2016). History, Development and Future of TRIGA research Reactors, Vienna

[47] **Wu, Z. & Williams,R.E.** (2015). Reactor Power Distribution Calculation in Research Reactors Using MCNP, *American Nuclear Society National Winter Meeting, Transactions of the American Nuclear Society,* Washington D.C

[48] **Loseille, A.** (2020). *Handbook of Numerical Analysis,* volume 21,Nort-Holland

[49] **Mavriplisa, D.J**.,(2000) Parallel Computational Fluid Dynamics, U.S.A: Elsevier Science Pages 57-72.

[50] **Patankar, S.** (1980). *Numerical Heat Transfer and Fluid Flow*,Washington: Hemisphere

[51] **Url-6** <https://www.afs.enea.it/project/neptunius/docs/fluent/html/ug/node470.html> Date Retrieved: 09.05.2020

[52] **Url-7** <https://www.afs.enea.it/project/neptunius/docs/fluent/html/ug/node279.htm#sec-material-functions> Date Retrieved: 09.05.2020

[53] **Url-8** <https://www.engineeringtoolbox.com/water-density-specific-weight-d_595.html.> Date Retrieved: 28.05.2020

[54] **Simnad, M.** (1980) The U-ZrHx alloy: Its properties and use in TRIGA fueL [INIS-US--09N0119] USA

[55] **Karriem, V.** (2011). *PSBR core design studies of the D2O tank design and new LEU fuel utilization*, (Master Thesis) The Pennsylvania State University, The Graduate School Department of Mechanical and Nuclear Engineering, Pensilvanya

[56] **Nukiyama, S.** (1996) The maximum and minimum values of heat Q transmitted from metal to boiling water under atmospheric pressure, *International Journal Heat and Mass Transfer*, 9:12, 1419-1433, doi:10.1016/0017-9310(66)90138-4

[57] **Url-9** <https://www.nuclear-power.net/nuclear-engineering/heat-transfer/boiling-and-condensation/natural-convection-boiling-onset-of-nucleate-boiling > Data Retrieved: 23.05.2020

[58] **Url-10** <https://www.engineeringtoolbox.com/water-vaporsaturation-pressure-d 599.html.> Date Retrieved: 23.05.2020

[59] **OECD** (2012), Nuclear Fuel Safety Criteria Technical Review (Second Edition), Nuclear Safety

APPENDICES

APPENDIX A: The data and codes used in CFD modelling.

APPENDIX B: Core modeling result tables and graphs.

APPENDIX A The data and codes used in CFD modelling

Table A.1 : Thermo-physical properties of water at atmospheric pressure.

Temperature (°C)	Density (kg/m^3)	Specific heat (J/kg K)	Thermal Conductivity (W/m K)
20	998.2	4183	0.5861
25	997.1	4183	0.5948
30	995.7	4183	0.603
35	994.0	4183	0.6107
40	992.2	4182	0.6178
45	990.2	4182	0.6244
50	988.0	4181	0.6305
55	985.7	4182	0.6360
60	983.2	4183	0.6410
65	980.6	4184	0.6455
70	977.8	4187	0.6495
75	974.9	4190	0.6530
80	971.8	4194	0.6562
85	968.6	4199	0.6589
90	965.3	4204	0.6613
95	961.9	4210	0.6634
100	958.35	4220	0.6651
110	950.95	4230	0.6676
120	943.11	4250	0.6691
140	926.13	4270	0.6697
160	907.45	4290	0.6694

```
#include "udf.h"
        DEFINE_PROFILE(heatflux_profileb1,thread,position)
{
real x[ND_ND];
real z;
face_t f;
#if RP_NODE

begin_f_loop(f,thread)
 {
  F_CENTROID(x,f,thread);
 z=x[2];
F_PROFILE(f,thread,position)=2.2721228e6*((-
1.3767*(z)*(z))+(2.6925*(z))-1.2454) ;
}
end_f_loop(f,thread)
#endif
}
```

Figure A.1 : The UDF example for the Heat-flux Thermal Boundary Conditions.

```
#include "udf.h"
DEFINE_SOURCE(energy_source_b1,c,t,dS,eqn)
{
real source;
real x[ND_ND];
real z;
#if PARALLEL
C_CENTROID(x,c,t);
z=x[2];
source=2.65226E+08*((-1.3767*(z)*(z))+(2.6925*(z))-1.2454);
dS[eqn]=0;
return source;
#endif
}
```

Figure A.2 : The UDF example for the volumetric heat source specification on fuel meat solid cell zone.

```
DEFINE_PROPERTY(cell_ktc_fuel, c, t)
{
  real ktc;
#if PARALLEL
  real temp = C_T(c, t);
    ktc=((12.5-2.4*(1-temp/1000)+1.5)* 1.730735) ;
#endif
  return ktc;
}
```

Figure A.3 : The UDF example for the temperature dependent material property.

APPENDIX B Core modeling result tables and graphs

Table B.1: Radial maximum temperature and average fuel temperature for all fuel elements.

Fuel Rod	Fuel Centerline Temperature (°C)	Max. Fuel Surface Temperature (°C)	Max. Clad Outer Temperature (°C)	Average Fuel Temperature (°C)
B1	238.364	194.050	180.912	170.427
B2	241.421	195.319	181.575	172.541
B3	235.177	191.736	178.327	167.329
B4	243.280	197.440	184.227	173.346
B5	227.246	184.711	172.611	162.308
B6	232.656	189.107	176.711	165.712
C1	215.954	176.079	164.158	155.586
C2	222.141	178.644	165.547	158.320
C3	212.753	172.375	160.475	153.448
C4	217.884	177.014	165.094	155.533
C5	205.480	167.867	156.927	148.122
C6	217.263	177.091	164.682	155.149
C8	208.996	170.119	158.874	149.337
C9	192.904	158.137	148.466	139.290
C10	200.322	163.674	152.767	143.446
C11	213.311	176.340	165.261	153.256
C12	214.283	173.443	160.918	152.751
D1	194.885	158.925	148.318	141.149
D2	195.054	159.532	148.402	140.421
D3	196.062	160.077	149.132	140.511
D4	206.759	170.026	159.057	149.029
D5	194.782	159.649	148.957	139.669
D6	188.134	153.451	143.002	136.125
D7	181.554	149.371	139.812	131.332
D8	175.160	144.765	135.278	127.084
D9	174.699	143.848	134.310	126.359
D10	181.303	151.484	142.437	131.572
D11	167.712	138.657	129.830	121.975
D12	164.199	137.269	128.752	119.681
D13	164.500	136.309	127.935	121.152
D14	167.164	137.945	129.073	121.449
D15	180.677	149.897	140.632	130.478
D17	193.375	159.380	148.848	139.124
D18	191.188	156.363	145.976	137.432

Table B.1(contd.): Radial maximum temperature and average fuel temperature for all fuel elements.

Fuel Rod	Fuel Centreline Temperature (°C)	Max. Fuel Surface Temperature (°C)	Max. Clad Outer Temperature (°C)	Average Fuel Temperature (°C)
E1	163.874	128.193	127.730	119.902
E2	236.004	176.464	176.464	167.943
E3	162.364	126.309	126.308	118.153
E4	171.964	134.366	134.365	125.318
E6	175.041	135.811	135.811	127.191
E7	162.803	125.967	125.967	118.160
E8	162.688	129.011	128.108	118.914
E9	159.524	126.522	126.207	117.040
E10	153.947	122.156	122.156	113.435
E11	150.191	118.159	118.159	110.136
E12	145.742	114.816	114.816	107.037
E13	141.206	114.514	114.398	105.140
E14	138.496	110.400	110.569	102.689
E15	138.536	110.464	110.464	102.870
E16	139.453	110.456	110.456	102.626
E17	140.292	113.448	113.292	104.243
E18	142.384	112.599	112.598	105.378
E19	144.646	114.572	114.572	105.977
E20	148.592	118.415	118.415	108.964
E21	162.214	128.254	128.254	118.748
E22	149.995	118.336	118.307	109.436
E23	156.164	123.032	123.031	113.644
E24	160.717	125.751	125.751	117.521
F1	133.409	108.463	108.463	98.800
F2	134.531	108.832	108.832	99.639
F4	129.743	103.823	103.823	96.216
F5	129.088	103.427	103.427	96.108
F6	154.038	122.465	122.465	113.037
F7	136.345	108.985	108.984	100.949
F8	135.475	107.482	107.482	99.618
F9	140.863	111.407	111.407	103.672
F27	116.883	94.889	94.257	87.803
F28	117.553	95.371	95.371	87.951
F29	125.849	101.761	101.575	93.599
F30	131.729	106.483	106.483	97.355

CURRICULUM VITAE

Name Surname: Feride KUTBAY

E-Mail: feride.kutbay@itu.edu.tr

EDUCATION:

B.Sc.: Nuclear Engineering Department, Engineering Faculty, Hacettepe University (2017).

PROFESSIONAL EXPERIENCE: Research Assistant

OTHER PUBLICATIONS, PRESENTATIONS AND PATENTS:

- **Kutbay, F.,** Allaf, M.A., Lule S.S. & Colak U. (2018). Doppler Broadening Effect on Reactivity Feedback in ITU Triga Mark II Research Reactor, *Proceedings of the International Conference Nuclear Energy for New Europe*, 206, September 10 – 13, 2018, Portorož, Slovenia.